RETHINKING GATING MECHANISM IN SPARSE MOE: HANDLING ARBITRARY MODALITY INPUTS WITH CONFIDENCE-GUIDED GATE

Anonymous authors
Paper under double-blind review

ABSTRACT

Effectively managing missing modalities is a fundamental challenge in real-world multimodal learning scenarios, where data incompleteness often results from systematic collection errors or sensor failures. Sparse Mixture-of-Experts (SMoE) architecture has shown the potential to naturally handle multimodal data, with experts specializing in different modalities. However, existing SMoE approaches often lack proper ability to handle missing modality, leading to performance degradation and poor generalization in real-world applications. We propose ConfSMoE to introduce a two-stage imputation module to handle the missing modality problem for the SMoE architecture by taking the opinion of experts and reveal the insight of expert collapse from gradient analysis with strong empirical evidence. Inspired by our gradient analysis, ConfSMoE proposed a novel expert gating mechanism by detaching the softmax routing score to task confidence score w.r.t ground truth signal. This naturally relieves expert collapse without introducing additional load balance loss function. We show that the insights of expert collapse empirically aligns with other gating mechanism such as Gaussian and Laplacian gate. The proposed method is evaluated on four different real world dataset with three distinct experiment settings to conduct comprehensive analysis of ConfSMoE on resistance to missing modality and the impacts of proposed gating mechanism.

1 INTRODUCTION

As modern applications increasingly involve data from multiple heterogeneous sources, multimodal learning has emerged as a critical paradigm to unlock complementary insights and enhance decision-making in complex tasks spanning medical decision support Zheng et al. (2024a;c), cross-modal inference Wu et al. (2017); Cheng et al. (2024), temporal reasoning Zheng et al. (2024b); Ni et al. (2024), and natural language understanding Fedus et al. (2022); Masoudnia & Ebrahimpour (2014). Sparse Mixture-of-Experts (SMoE) architectures Yao et al. (2024); Yun et al. (2024); Mustafa et al. (2022) are widely used in multimodal learning for their ability to assign different experts to different input patterns through conditional computation. They are particularly effective when all input modalities are present, enabling diverse feature extraction and flexible expert routing. However, this assumption is often violated in practice. Incomplete modality observations are common in real-world scenarios due to sensor failures, privacy restrictions, or heterogeneous data collection pipelines Yun et al. (2024); Sun et al. (2024); Shang et al. (2017); Wang et al. (2023). When one or more modalities are missing, SMoE models receive partial input signals, which undermines the reliability of the gating mechanism and results in suboptimal expert selection. Although some methods attempt to assign different modality combinations to designated experts Han et al. (2024); Yun et al. (2024), this strategy becomes computationally intractable as the number of modalities grows exponentially. To reduce this complexity, recent SMoE frameworks typically activate the Top-K experts per sample. However, the use of softmax-based routing Fedus et al. (2022) tends to produce sharp distributions, often concentrating the routing on a single expert. This leads to the expert collapse problem Fedus et al. (2022); Han et al. (2024); Yun et al. (2024), where only a few experts dominate the computation as shown in Figure 1a, resulting in poor diversity and limited generalization. Efforts to mitigate this issue using load-balancing losses introduce additional optimization challenges. In particular, they may cause unstable or ambiguous expert selection during training, as illustrated in Figure 3a.

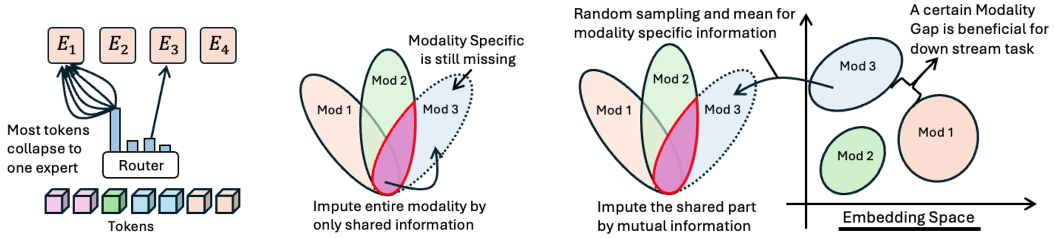
E_1
E_2
E_3
E_4
Most tokens collapse to one expert
Router
Tokens
Modality Specific is still missing
Mod 1
Mod 2
Mod 3
Impute entire modality by only shared information
Random sampling and mean for modality specific information
A certain Modality Gap is beneficial for down stream task
Mod 1
Mod 2
Mod 3
Impute the shared part by mutual information
Mod 3
Mod 1
Mod 2
Embedding Space

(a) Expert Collapse (b) Imputation by shared (c) Ours

Figure 1: Expert Collapse of MoE and Comparison with Two Different Modality Imputation

In addition, recent works Fedus et al. (2022); Han et al. (2024); Yun et al. (2024) has tackled expert collapse within SMoE architectures, handling missing modalities remains an orthogonal and unresolved challenge. In the context of missing modalities, many recent approaches aim to reconstruct absent views through cross-modal information sharing Ma et al. (2021); Wang et al. (2023); Yao et al. (2024) as shown in Figure 1b. However, these methods typically introduce multiple auxiliary losses to jointly learn task-relevant, shared, and modality-specific features, which increases training complexity and may inadvertently erode modality-unique information. To alleviate this issue, recent work has proposed using learnable modality banks Yun et al. (2024) to impute missing inputs based on the available modality combinations. Nevertheless, such banks are usually initialized randomly, similar to prompt tuning Jia et al. (2022); Lester et al. (2021), and often fail to capture fine-grained modality-specific structure, limiting their effectiveness in practical settings.

To overcome the limited robustness of existing SMoE models under incomplete modality conditions, we propose a two-stage imputation approach based on a core insight: *a complete modality imputation should consist of modality- and instance-specific information*, a property often overlooked in prior work. Firstly, we estimates missing modalities using intra-modality correlations, empowering modality-specific information, and then refines these estimates through token-level cross-modal alignment to existing modality of the same sample, empowering instance-specific information. This refinement leverage the advantages of MoE that the data used to refine missing modality are from different opinion of experts. This approach is inspired by the modality gap phenomenon discussed by Liang et al. (2022) and illustrated in Figure 1c, which suggests that a certain level of discrepancy between modalities is both expected and beneficial for downstream tasks. Thus, it is natural to first impute missing modalities using intra-modality information subsequently enhance them through token-level cross-modal refinement to add up instance-specific feature from available modality.

We further uncover and formalize a critical cause of expert collapse in SMoE: the gradient concentration induced by softmax gating, which suppresses routing diversity and limits generalization Fedus et al. (2022); Wang et al. (2024); Yun et al. (2024); Han et al. (2024); Chi et al. (2022). Through gradient analysis, we show that conventional load-balancing losses exacerbate this issue by introducing gradient conflicts during optimization, reflecting by the "Sinoual Wave" pattern in expert selection plot shown in Figure 3a. To resolve this, we design a *confidence-guided expert routing mechanism* that replaces softmax gating with token-level confidence scores. This formulation not only avoids the adverse effects of entropy-based balancing but also enables stable, interpretable expert selection. The two mechanisms handling missing modality and Confidence-guided gating consist of our final proposed method: **ConfSMoE**. By decoupling routing score from the optimization bottlenecks of prior designs, ConfSMoE achieves both enhanced expert diversity and consistent performance across a wide range of incomplete modality scenarios. Our contributions are the following:

- A confidence-guided expert routing mechanism is proposed to mitigate expert collapse by decoupling gating from softmax-induced sharpness. Token-level confidence is used as a interpretable signal for expert selection.
- A two-stage imputation framework is developed, where missing modalities are first reconstructed using modality-specific patterns, then refined with instance-level cross-modal context to preserve structural fidelity.

- Empirical results across three missing-modality settings demonstrate strong robustness and generalization. Performance improvements are further supported by ablation studies that align with theoretical analysis.

2 Preliminaries

2.1 Mixture-of-Expert Architecture

In this work, we build upon the SMoE framework by incorporating expert routing into the Transformer's feedforward layers, enabling dynamic token-to-expert assignment based on learned routing scores. This architecture supports selective expert activation, where only the Top-K experts are engaged per token, and proves especially effective in the joint expert setting Han et al. (2024), allowing tokens from different modalities to be routed to shared experts for enhanced cross-modal interaction. We begin with the standard Softmax SMoEs with N number of expert as a baseline configuration. Denote that input token embedding $\mathbf{h} \in \mathbb{R}^d$ and the a learnable softmax router $G(\mathbf{u}) = \frac{\exp(u_i)}{\sum_j^d \exp(u_j)} = \mathbf{g} = [g_1, g_2, \dots, g_N]$, where $\mathbf{u} = \mathbf{W}_r\mathbf{h}$ and $\mathbf{W}_r \in \mathbb{R}^{N \times d}$ is the weight of router to linearly map $\mathbf{h}$ to gating logits $\mathbf{u} \in \mathbb{R}^N$. $G(\mathbf{u})$ produces routing score g_i for each expert E_i from expert pool $\mathbf{E} = [E_1, E_2, \dots, E_N] \in \mathbb{R}^{d \times d}$. We consider the Top-K operation as a binary mask $\mathbf{m} \in \{0, 1\}^N$ to select the Top-K experts in forward as shown in Eq. 1. The final tokens/samples representation is weighted summation from Top-K experts with corresponding routing score g_i. Formally, we can represent the forward process of SMoE as in Eq. 2:

$$\mathbf{m} = \text{Top-K}(\mathbf{g}, K) = \mathbf{1}\{\text{if } g_i \text{ is in the top K element of } \mathbf{g}\} \tag{1}$$

$$f(\mathbf{h}) = \mathbf{h} + \sum_{i=1}^{N} m_i g_i E_i(\mathbf{h}) \tag{2}$$

2.2 What Causes Expert Collapse?

The Jacobian matrix of Eq. 2 w.r.t $\mathbf{h}$ can be analyzed to reveal the underlying cause of expert collapse in SMoE. Therefore,

$$\mathbf{J}_{MoE} = \sum_{i=1}^{N} m_i \frac{\partial g_i}{\partial \mathbf{h}} E_i(\mathbf{h}) + \sum_{i=1}^{N} m_i g_i E_i^{'}(\mathbf{h}) \tag{3}$$

Note that expert $E_i(h)$ and softmax gating $G(\mathbf{u})$ themselves are differentiable w.r.t $\mathbf{h}$ and the mask $\mathbf{m} = \text{Top-K}(\mathbf{g}, K)$ is a piecewise-constant mask that only changes when the ordering of routing score $\mathbf{g}$ changes. Conditioning on a fixed mask $\mathbf{m}$, Eq. 2 reduces to a linear combination of differentiable functions (e.g. $E_i(h)$ and $G(\mathbf{u})$), where the gradient will only propagate through the terms with $m_i = 1$, enabling parameter update for those activated experts. Consequently, during training, only the selected experts are differentiable. Therefore, we can denote the Jacobian of softmax as $\mathbf{J}_{softmax} \in \mathbb{R}^{N \times N}$, where each entry $\mathbf{J}_{softmax}^{i,j} = g_i(\delta_{ij} - g_j)$ and δ_{ij} is Kronecker delta. In matrix form, Jacobian of softmax is $\mathbf{J}_{softmax} = \textbf{diag(g)} - \mathbf{g}\mathbf{g}^{\top}$ and the Top-K $\mathbf{J}_{softmax} = \mathbf{m}(\textbf{diag(g)} - \mathbf{g}\mathbf{g}^{\top})$. Therefore, we can rewrite Eq. 3 to Eq. 4: In first term, only those experts with higher gating score will be chosen and the gradient is backward in $\textbf{diag(g)} - \mathbf{g}\mathbf{g}^{\top}$ to learn better routing score. In second term, the gradient is backward to those selected experts E_i to learn better representation. During training, experts that receive more updates tend to be selected more frequently, as their improved representations attract higher gating scores. *This creates a feedback loop which those experts with more expressive power will lead to higher gating score and thus more updates on weight for strong expressive power, resulting a sparse resulting expert collapse based on token preference and produce rich-get-richer expert.*

$$\mathbf{J}_{MoE} = \underbrace{\mathbf{E}(\mathbf{h})\mathbf{m}(\mathbf{diag}(\mathbf{g}) - \mathbf{g}\mathbf{g}^\top)}_{\text{Learning a better routing score}} \quad + \quad \underbrace{\sum_{i=1}^{N} m_i g_i E_i^{'}(\mathbf{h})}_{\text{Learning a better representation}} \tag{4}$$

2.3 Gradient of Load Balance Loss

This expert collapse phenomenon restrict the model learning capacity since many other experts are wasted and can not reflect the actual expert diversity. One widely-used solutions to achieve balance expert usage is to introduce additional load balance loss Yun et al. (2024); Han et al. (2024). However, such load balance loss approach is difficult to optimize since it produces gradient direction opposite to routing score term in Eq 4. To show this, we consider that any load balance loss $\mathcal{L}_{load}$ will eventually result a diverse softmax routing distribution, which encourage higher entropy on the routing score distribution. From **Assumption** 1 defined in Appendix, we define that the objective of any $\mathcal{L}_{load}$ as $\frac{1}{\mathcal{H}(\mathbf{g})}$ over the softmax distribution, where $\mathcal{H}(\mathbf{g}) = -\sum_i^N g_i log\ g_i$ represent the entropy of softmax distribution $\mathbf{g}$. Taking the Jacobian over the $\mathcal{L}_{load}$ will give us (See detailed in Appendix. B.2):

$$\mathbf{J}_{load} = [\frac{1}{\mathcal{H}(\mathbf{g})^2}(log(\mathbf{g}) + 1)^\top] \cdot (\mathbf{diag}(\mathbf{g}) - \mathbf{g}\mathbf{g}^\top) \tag{5}$$

Recall that $\mathbf{E}_K(\mathbf{h})$ in Eq.4 is a set of expert with ReLU activation, we assume this network should not output negative value as activation is located on positive side. We also know the fact that the Jacobian of softmax $\mathbf{J}_{softmax}$ is symmetry and always Positive Semi-Definite (PSD) Gao & Pavel (2017), making the optimization direction of better routing score is always positive as the eigen-values are positive. In contrast, $log(\mathbf{g}) + 1 = [log(g_1) + 1, log(g_2) + 1, \ldots, log(g_N) + 1]$. When sharp distribution appears, only one g_j is closed to 1 while other $g_i, (i \neq j)$, are closed to 0. Therefore, $\frac{1}{\mathcal{H}(\mathbf{g})^2}(log(\mathbf{g}) + 1)^\top$ is exponentially dominated by negative value, producing conflict gradient between $\mathbf{J}_{load}$ and the first term of $\mathbf{J}_{MoE}$. The Top-K operation does not change PSD property of first term in Eq.4, but the gradient will be backward through the term where $m_i = 1$ in J_{MoE}. In addition, we notice that first term gradient of Eq. 4 is only impacted by the Top-K g_i while the gradient in Eq. 5 is dominated by the Top-K g_i. The shaper the gating score distribution is, the more gradient conflict will be. It is also worthy to notice that gradient in Eq.5 conflict occurs for any Top-K selection as the load balance loss consider all g_i regardless of number K expert selection. Taking an extreme example, Top-1 selection Fedus et al. (2022) generates one g_i out of $\mathbf{g}$ for the second term of Eq.4 while Eq.5 still take all g_i to gradient computation in practice. Therefore, *the opposite gradient from axillary load balance loss makes the training difficult to converge to global minimum and Expert selection becomes ambiguous, failing to reflect actual capacity of expert.*

3 Propose Method

3.1 ConfNet:Confidence-Guided Gating Network

From Eq. 5 and Eq. 4, we understand that load balance loss produce opposite gradient to softmax router in typical SMoE. To avoid this gradient conflict and balance the load, the potential solution is to remove the association of sharp distribution from Eq. 4 and attempt to implicitly achieve load balance. One is to replace the routing function as illustrated in Figure. 2 (c) and one is to decouple the gating score with softmax router as illustrated in Figure. 2 (d). A typical example from a recent work, FuseMoE Han et al. (2024), they replace the Softmax router to Laplacian router and calculate the routing score based on similarity of the expert embedding by $\mathcal{L}_1$ distance. Then, the Top-K experts are selected with highest similarity to expert embedding and Laplacian router is not a sharp distribution so that the load shows implicit balance pattern as in Appendix Figure 8. The second approach is to decouple the connection of gating score and softmax distribution. One simple approach is to consider all expert equally important, then the final representation is averaged from all selected expert. However, this averaged approach does not emphasize the difference of expert and lose the specification of expert.

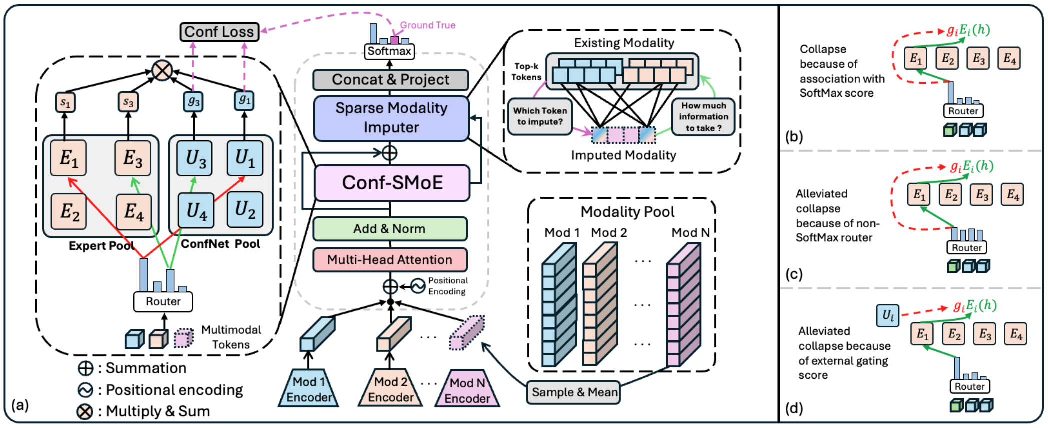

Figure 2: The Framework of ConfSMoE: (a) ConfSMoE considers the confidence learned from ConfNet pool as the gating score for expert aggregation. The ConfNet pool is a set of one-layer linear weight $\mathbb{R}^d \to \mathbb{R}^1$. Missing modality imputation is achieved by taking the mean of random instances from the corresponding modality of training data as common modality specific feature. The instance-specific feature are sparsely aggregated from existing modality. (b) Sharp gating score causes expert collapse. (c)(d) "Fair" gating score distribution and decoupling gating score can alleviate the expert collapse without the helps of load balance loss.

Therefore, we propose a Confidence-Guided Gating Network Pool (ConfNet), which introduces a novel routing strategy guided by task confidence. Specifically, instead of solely relying on conventional softmax-based gating, which often results in sharp distributions and entangled gradient contributions, ConfNet leverages the ground-truth label information to supervise the routing mechanism, encouraging expert selection aligned with task-relevant confidence rather than token or embedding similarity as in Han et al. (2024); Fedus et al. (2022). For each expert $E_i : \mathbb{R}^d \to \mathbb{R}^d$, we introduce an auxiliary confidence estimation network: a one-layer linear network $U_i : \mathbb{R}^d \to \mathbb{R}^1$ that maps token embedding $\mathbf{h} \in \mathbb{R}^d$ to a single scalar logits $v_i \in \mathbb{R}^1$. v_i is then mapped to a confidence score $c_i \in (0, 1)$ as gating score by Sigmoid, representing the confidence of ground truth label y_t. To learn the ground true confidence p_t of downstream task w.r.t y_t, where y_t is ground truth label. We apply MSE loss as an axillary loss that minimize the difference between c_i and p_t. Formally, given any classification dataset D with supervised signal y_i and number of instance $|D|$, we consider the task loss $\mathcal{L}_{task}$ as Cross Entropy Loss and the final objective is to optimize:

$$\mathcal{L} = \mathcal{L}_{task} + \mathcal{L}_{conf} = \frac{1}{|D|} \sum^{|D|} y_t log(p_t) + \frac{1}{|D|K} \sum^{|D|} \sum_{i=1}^{N} m_i(c_i - p_t)^2 \tag{6}$$

Note that Eq. 6 is convex as both cross-entropy and MSE loss are well-known convex. During both training and inference, c_i serves as a proxy gating score for each expert to token fusion in Eq. 3. The c_i is Token-level confidence, which each token has one corresponding c_i for aggregation as in $\sum_{i=1}^{N} m_i g_i E_i(\mathbf{h})$ as in Eq. 2, resulting in a variant of proposed method for fine-grained feature learning, denoted as ConfSMoE-T. Additionally, a expert-level gating signal is also implemented for coarse-grained information retrieval. We aggregate token-level representations assigned to each expert and average them to compute expert-level gating signals as expert-level variant, denoted as ConfSMoE-E in experiment. The multimodal interaction is learned during the token assignment for all experts, which all modalities are shared one identical expert pool. This confidence-driven routing enables both fine-grained specialization and robust multimodal interaction, leading to improved generalization and interpretability.

3.2 Missing Modality Modeling: Two-Stage Imputation

Inspired by the modality gap phenomenon observed in contrastive learning Liang et al. (2022), we hypothesize that a similar gap exists in our multimodal setting, and it may contribute positively to model performance, as illustrated in Appendix Figure 4. The presence of this modality gap suggests that imputing a missing modality using only shared information from the available modalities is inherently challenging, due to the distinct representational spaces each modality occupies. Ideally, the imputed modality should preserve the characteristics of its original distribution without being significantly biased by other modalities. To address this, we propose a **Two-stage Imputation** strategy to first reconstruct the representative feature from the missing modality distribution itself, and further refine the pre-imputed modality by adding instance-specific feature from the available modalities.

Pre-Imputation: To retrieve modality-specific feature, given a sample x_i with missing modality $M_m \in \mathbb{R}^{s\times d}$ and arbitrary available modality $M_a \in \mathbb{R}^{s\times d}$, where s is the sequence length. Pre-imputation aims to obtain the modality-specific feature from other instances of M_m distribution. One typical way is to take the mean feature distribution of M_m, but simply taking the mean may be overfitting to training set and all representation across different modality samples will be deterministic and uninformative. In contrast to mean representation, we wish to introduce some stochasticity during the pre-imputation as this stochasticity may prevent the representation to collapse to the same representation. Specifically, we generate an pre-imputed modality embedding $\bar{M}_m$ by sampling n number of instances out of b number of instances in modality pool $M_{m,i} = [M_{m,1}, M_{m,2}, \cdots, M_{m,b}]$ as follows:

$$\bar{M}_m = \frac{1}{n}\sum_{i=1}^{n} \mathbf{1} M_{m,i} \tag{7}$$

Where $\mathbf{1} \in \{0,1\}^b$ is the selection vector for M_m and $\mathbf{1}_i = 1$ represents the i-th instance from the modality pool that is selected. $\bar{M}_m$ will be sent to ConfSMoE to learn the interaction between different modalities. We denoted M_m^* as the pre-imputed modality representation after ConfSMoE and M_a^k as the available modality representation returned from k-th expert.

Post-Imputation: To refine M_m^* by available modality, we proposed a post-modality imputation to further capture the interactions between available and missing modality. Unlike conventional approaches that solely rely on the shared representation from individual network, our method leverages information from various experts by selectively incorporating tokens. This allows the model to absorb nuanced, instance-specific features and interaction between modalities from different views of expert to available modality. We employ a sparse attention mechanism, under the assumption that only a subset of modality-specific information is meaningfully shared across M_a^k. By enforcing sparsity, the model is encouraged to attend to the most relevant parts of the available modalities, thereby reducing the risk of injecting modality-irrelevant or noisy information into the imputed representation. Recall from Eq. 2, Top-K MoE generate K specialized representation from available modality $M_a^k \in \mathbb{R}^{s\times d}$, $k = 0, 1, \ldots K$. Then, we concatenate all the M_a^k returned from K expert to form a representation of the opinion of different experts, denoted as $M_a^* \in \mathbb{R}^{(s\times K)\times d}$. We apply a sparse cross-attention over M_m^* and M_a^* to select the most relevant tokens to refine $M_m^* \in \mathbb{R}^{s\times d}$. The SparseCrossAttention takes M_m^* as Query modality $\mathbf{Q}_m = \mathbf{W}_q M_m^*$, M_a^* as Key modality $\mathbf{K}_a = \mathbf{W}_k M_a^*$ and Value modality $\mathbf{V}_a = \mathbf{W}_v M_a^*$, where $\mathbf{Q}_m \in \mathbb{R}^{s\times d}$ and $\mathbf{K}_a, \mathbf{V}_a \in \mathbb{R}^{(s\times K)\times d}$. Note that $\mathbf{W}_q, \mathbf{W}_k, \mathbf{W}_v$ are shared between all modalities. Then, we obtained the cross-attention score $\mathbf{A}_a \in \mathbb{R}^{s\times(s\times K)}$ from the dot product of $\mathbf{Q}_m$ and $\mathbf{K}_a$. Then, we apply a binary mask $\mathbf{t}$ on the attention scores $\mathbf{A}_a$ to retain only the Top-T entry based on the rank of the attention score (1 indicate presence) alongside the dimension of $\mathbf{K}_a$, producing a sparse attention map $\mathbf{A}_a^*$. $T = \frac{s(|M|-1)}{B}$, where $|M|$ represents the number of modality in dataset and B is a sparsity hyperparameter, we set B as 4 by default.

$$\mathbf{t} = \text{Top-T}(\mathbf{A_a^*}, T) = \mathbf{1}\{\text{if } A^*_{a,i} \text{ is in the top T element of } \mathbf{A_a^*}\} \tag{8}$$

$$\mathbf{A}_a^* = \mathbf{t} \odot softmax(\frac{\mathbf{Q_m K_a}^\top}{\sqrt{d}}) \in \mathbb{R}^{s\times(s\times K)} \tag{9}$$

Thus, we aggregate the value matrix $\mathbf{V}_a$ using the sparse attention weights $\mathbf{A}^*$ to obtain the output of $SparseCrossAttention$ (SCA). When multiple available modality M_a^* are presented in the dataset, we compute their contributions individually and sum them to refine M_m^*:

$$M_m^* = LayerNorm\left(M_m^* + \sum^{|a|} SCA(M_m^*, M_a^*, M_a^*)\right) = LayerNorm\left(M_m^* + \sum^{|a|} \mathbf{A}_a^* \mathbf{V}_a\right) \tag{10}$$

In addition, we expect this refinement to redistribute the representation of M_m^* instead of generating large-scale representation and lead to diverge training. A LayerNorm layer is applied to scale the feature map back to consistent distribution as in other layers. With SCA, the post-imputation serves as a refinement module to add an instance-specific feature to M_m^*, which each modality can contribute differently on different subsegment representations of M_m^*. We visualize the attention weights after imputation in the Appendix Figures 14, 15, and 16, showing that the query modality can dynamically adjust the significance of information by leveraging both expert specialization and shared cross-modal cues, given that attention maps reveal distinct weight distributions across different modalities and experts.

4 Experiment

4.1 Experiment Setting

To ensure a fair comparison with baseline methods, we adopt the best-performing hyperparameter settings reported in their respective papers and official implementations. Additionally, we standardize the hidden dimension to 128 across all models. To eliminate confounding effects introduced by varying encoder architectures, we use the same modality-specific encoders for all models, as differences in encoder design can significantly influence final performance. For the MIMIC-III and MIMIC-IV datasets, we employ a pretrained ClinicalBERT Alsentzer et al. (2019) for textual data, a one-layer patch embedding module for both irregular time series and ECG signals, and a pretrained DenseNet Cohen et al. (2022) from TorchXRayVision for chest X-ray (CXR) images. **Experiment Setting I: Natural Missing Modality**. This setting reflects real-world missingness patterns observed in clinical datasets. **Experiment Setting II: Random Modality Dropout**. A fixed percentage of modalities are randomly dropped for each instance, while ensuring that each instance retains at least one modality in both train and test set. **Experiment Setting III: Asymmetric Modality Dropout**. Half of the modalities are randomly dropped during training, while testing is performed with only one or two modalities present per instance, simulating domain shifts or deployment constraints. All experiments are 3-Fold cross-validate in different seeds for fair comparison.

4.2 Primary Results

Experiment Setting I: In Table 1 and Appendix Table 7, we provide the experiments results on experiment setting I for three different ICU benchmarking task, where the modalities are natural missing instead of random. We obtain the following observations from the results: (1) In clinical benchmarking tasks 48-IHM, LOS, and 25-PHE, our proposed methods can significantly outperform the most recent baseline approaches such as FuseMoE and FlexMoE and other tradidtional multimodal learning methods in terms of F1 and AUC score. For MIMIC-III, the improvement on F1 and AUC is ranging from 1.81% to 3.91% and 0.92% to 1.22% respectively. (2) The improvement is even further when the size of dataset scale to bigger dataset but the same domain like MIMIC-IV. The improvement on F1 and AUC is ranging from 1.37% to 4.12% and 1.96% to 4.85%. The above empirical evidence roots and supports our claims that the model is strongly robust to missing modality and learn more comprehensive understanding on multimodal inputs.

Table 1: Experiment setting I: Main results on MIMIC-IV

Task	Metric	SMIL	ShaSpec	mmFormer	TF	LlMoE	FuseMoE-S	FuseMoE-L	FlexMoE	**ConfSMoE-T**	**ConfSMoE-E**
48-IHM	F1	39.58 ± 1.12	32.97 ± 1.08	45.39 ± 1.60	11.60 ± 0.54	43.76 ± 0.44	30.14 ± 1.15	40.21 ± 1.29	35.29 ± 0.30	**49.18 ± 0.22**	48.32 ± 0.30
	AUC	76.60 ± 0.98	78.29 ± 0.25	80.43 ± 0.76	67.08 ± 0.77	82.97 ± 0.61	71.34 ± 0.88	78.05 ± 0.72	80.45 ± 0.44	**85.24 ± 0.10**	85.09 ± 0.17
LOS	F1	58.52 ± 0.44	56.22 ± 0.28	57.06 ± 0.32	42.01 ± 1.12	59.03 ± 0.39	57.59 ± 0.76	58.31 ± 0.46	56.96 ± 0.53	61.33 ± 0.39	**61.35 ± 0.41**
	AUC	75.86 ± 0.66	72.22 ± 0.18	74.65 ± 0.32	64.11 ± 0.40	76.17 ± 0.17	72.59 ± 1.07	72.59 ± 0.61	74.81 ± 0.37	**78.22 ± 0.15**	77.85 ± 0.12
25-PHE	F1	27.77 ± 0.91	25.53 ± 0.11	26.15 ± 0.12	26.52 ± 0.29	25.38 ± 0.52	12.45 ± 0.54	12.25 ± 0.55	24.61 ± 0.71	**28.67 ± 0.33**	28.54 ± 0.25
	AUC	63.90 ± 1.31	62.57 ± 0.23	70.33 ± 0.12	56.28 ± 0.16	72.50 ± 0.67	55.48 ± 0.39	58.52 ± 0.27	71.57 ± 0.47	**74.56 ± 0.19**	74.42 ± 0.34

Experiment Setting II: In Appendix Table 8 and Table 9, we implement Random Modality Dropout to study the sensitivity of model to missing modality. In this setting, we empirically find that those methods with missing modality imputation usually shows higher tenacity in high proportion of missingness such as FlexMoE and our propose method. Although ShaSpec has also impute the missing modality by shared information, but it is weak on the backbone model and struggling to optimize with multi-task objectives. Our proposed method, on the other hand, shows superior performance across all setting in CMU-MOSEI and CMU-MOSI for all metrics.

Experiment Setting III: In Appendix Table 10, Table 11, Table 12 and Table 13, we study which modality combination is significant and how is the tenacity of our proposed method to different distribution shift on missing modality. We find that single modality shows very similar performance during inference phrase in our proposed method and Flex-MoE across AUC and F1, indicating the effectiveness of missing modality imputation. In particular, our proposed also shows the highest resistance to missing modality across different combination and remains competitive performance no matter what modality is missing. In addition, the modality combination Audio-Video is the worse modality combination for all implemented models. The potential reason may be that the data interaction between those two modalities are weak or even opposite. We show some visualization evidence in Figure 4 that the embedding of those two modalities are mostly symmetry.

4.3 Why Does Confidence-Guided Gating Improve Performance?

We implemented experiment on switching different gating mechanisms in our propose method as shown in Table 2 and plot the expert selection heatmap in Appendix G. Figure 5 illustrates the softmax gating mechanism without load balance regularization, which exhibits severe expert collapse where only a few experts are consistently selected throughout training. Although load balance is adapt to distribute the load, it is hard to learn proper routing scores since the optimization is opposite as stated in Section 2, leading to suboptimal solution in this ablation. Softmax w/ $\mathcal{L}_{load}$ variant shows "Sharp Sinusoidal Wave" expert selection pattern as shown in Figure 3a, indicating the selection is ambiguous and difficulty on convergence. We also found that considering the uniform weight for all experts can achieve similar performance as sole softmax and generate similar sinusoidal pattern as softmax w/ $\mathcal{L}_{load}$, shown in Figure 9.

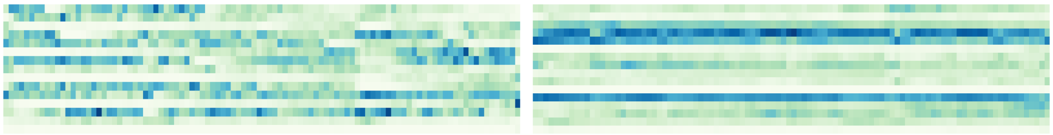

(a) Expert selection of softmax w/ $\mathcal{L}_{load}$

(b) Expert selection of ConfNet

Figure 3: Expert selection: X-axis represents epoch and Y-axis represents expert ID. The darker the color, the more selection will be for a particular expert. See detailed and more plots in Appendix G

Table 2: Ablation I: Different router. CMU-MOSI adopt 50% missing setting in Experiment III

Task	Metric	Mean	Softmax	Softmax w/ $\mathcal{L}_{load}$	LFB	Gaussian	Laplacian	**ConfNet**
MIMIC-III	F1	48.34 ± 0.22	48.59 ± 1.97	51.67 ± 0.62	48.36 ± 0.88	46.50 ± 1.62	50.10 ± 1.17	**53.44** ± **0.27**
	AUC	85.13 ± 0.16	85.91 ± 0.84	85.97 ± 0.52	85.05 ± 0.67	86.70 ± 0.33	85.47 ± 1.05	**87.05** ± **0.58**
CMU-MOSI	F1	42.29 ± 0.87	41.47 ± 0.94	42.43 ± 1.34	43.86 ± 0.56	42.57 ± 1.81	43.15 ± 1.53	**44.34** ± **0.77**
	AUC	68.01 ± 1.68	68.77 ± 1.66	67.40 ± 0.54	66.60 ± 2.24	67.74 ± 0.45	67.60 ± 1.54	**70.41** ± **1.31**

In addition, Laplacian Han et al. (2024) and Gaussian gating Han et al. (2024); Xu et al. (1994) function can achieve comparable to softmax w/ $\mathcal{L}_{load}$ gating mechanism without helps of $\mathcal{L}_{load}$, providing further evidence to support the advantage of balance expert selection. Our proposed ConfNet without helps of $\mathcal{L}_{load}$ is the best and significantly outperform other gating function in CMU-MOSI and MIMIC-III. As illustrated in Figure 6 and supported by the quantitative results in Table 2, ConfNet not only preserves expert specialization but also achieves better load balancing than Laplacian, albeit slightly less balanced than softmax with $\mathcal{L}_{\text{load}}$ and Gaussian gating as shown in Appendix G. This comparison provides two insights: First, optimization of $\mathcal{L}_{load}$ is simply against to optimization of softmax gating score but does not help to identify the best expert, reflecting the

"Sharp Sinusoidal Wave" pattern in expert selection and ambiguous expert selection. Second, learning specialization of expert can also benefit to downstream performance. Notably, both ConfNet and Laplacian gates demonstrate a common pattern: *they maintain the specialization of dominant experts while redistributing some load to less active ones*, which highlights that strict load balancing may suppress expert specialization and degrade performance, whereas maintaining a balance between specialization and load distribution leads to superior results. We provide further explanation in Appendix G for supporting our claims.

4.4 How ConfNet and Modality Imputation integrate together?

Table 3: Ablation II: Module dropout. CMU-MOSI adopt 50% missing in Experiment II

Variants	MIMIC-III		CMU-MOSI	
	F1	AUC	F1	AUC
w/o Conf	48.59 ± 1.97	85.91 ± 0.84	42.47 ± 0.94	68.77 ± 1.66
w/o impute	49.59 ± 0.29	86.31 ± 0.12	42.46 ± 2.29	68.44 ± 1.82
w/o post-impute	49.86 ± 1.89	86.53 ± 0.10	43.14 ± 1.32	69.13 ± 1.45
w/o impute & Conf	46.32 ± 1.66	85.15 ± 0.57	41.98 ± 0.74	68.48 ± 1.90
ConfSMoE-T	53.44 ± 0.27	87.05 ± 0.58	44.34 ± 0.77	70.41 ± 1.13

We implement the experiment in Table 3 by removing ConfNet and the two-stage imputation module gradually. This experiment demonstrates that both novel modules, ConfNet and the two-stage imputation, are effective on their own, while their integration provides strong robustness against the missing modality challenge. Specifically, ConfNet captures informative features from the imputed modality, and the adaptive two-stage imputation operation reconstructs high-quality features, thereby complementing each other to achieve robust performance. Specifically, we dropped the entire imputation module and keep the missing modality as zeros (w/o impute), we can see that F1 and AUC dropped off by 3.85 and 0.74 on MIMIC-III, 1.88 and 1.97 on CMU-MOSI. This performance drops is even worse when imputation and ConfNet gating mechanism is removed from proposed method, providing strong empirical evidence for effectiveness of our design. We further remove the post-imputation (w/o post-impute) and observe that ConfNet can still take advantage of modality-specific feature for their downstream task, showing robustness against missing modality.

4.5 Complexity Analysis

In Table 14, we control the number of parameters in three different scales to compare performance. We aims to find the best model given similar parameter and computational costs. Although ShaSpec and TF achieve lower FLOPs given the same parameter amount, their performance remains less competitive than most Transformer- and MoE-based models. Among MoE-based models, ConfSMoE-T delivers the best performance while maintaining similar MFLOPs and parameter counts to the second-best baseline. Under comparable parameter settings, LIMoE and mmFormer fail to keep FLOPs as low as ConfSMoE-T and yield suboptimal results. Moreover, LIMoE is particularly inefficient, as its MFLOPs are substantially higher than those of other models with similar parameter sizes. By increasing the number of parameter to a larger scale, we can observed different amount of increment across the selected models while none of baseline can archive the same performance as ConfSMoE-T. Many baselines are still less competitive to small scale ConfSMoE-T, demonstrating the scalability of ConfSMoE.

5 Related Works

While in many works considers that the interaction between multimodal data can bring comprehensive understanding for downstream task. Initial multimodal fusion approach usually incoperates neural kernel fusionBucak et al. (2013); Poria et al. (2015), early/late network fusion Xu et al. (2023); Baltrušaitis et al. (2018); Guo et al. (2019). Approaches such as Tensor Fusion NetworkZadeh et al. (2017), Multimodal TransformerTsai et al. (2019) and Multimodal Adaption GateRahman et al. (2020), LIMoEMustafa et al. (2022) all highlights the multimodal interactions are beneficial to downstream task. In medical domain, MedFuse Hayat et al. (2022) incorporated CXR and EHR modality to jointly fuse modality with early and later fusion in a single fusion network. MISTS Zhang et al. (2023) incorporated multi-time attention mechanism to encoder irregular time serires and adapts multimodal cross attention to fuse two different modality. Yang & Wu (2021) fused multimodal data in a attention gate and compute a replacement vector for modality fusion. However, these approaches are limited to full modality only and difficult to extend to increasing number of modality. Missing modality is realistic and practical problem in real life application such as medical diagnose. SMIL

Ma et al. (2021) proposed a Bayesian meta-learning solution with reconstruction network to impute the missing modality from in hidden state during fusion. Du et al. (2018); Shang et al. (2017) propose generative adversarial networks to impute the missing modality by semi-supervised learning. ShaSpec Wang et al. (2023) and DrFuse Yao et al. (2024) designed multiple loss function to learn share and specific representation of different modality. However, the reconstruction network from SMIL and ShaSpec requires multiple additional auxiliary loss function, which occupies the great amount of gradient in optimization process instead of task specific loss. Sun et al. (2024) In addition, recent studies like FuseMoE Han et al. (2024) respect the missingness of modalities and wish to assign each combination of multimodal data to different experts. Flex-MoEYun et al. (2024) further expand the advantages of FuseMoE and introduce a modality bank to impute the missing modality.

6 Conclusion

In this work, a novel ConfSMoE model, a confidence-guided sparse mixture-of-experts framework, is proposed to robustly handle multimodal learning with missing modalities. We proposed two key innovations: a two-stage imputation strategy that preserves modality-specific structure, and a novel confidence-driven gating mechanism that decouples expert selection from softmax-induced sharpness. These components jointly improve both expert specialization and routing stability without requiring entropy-based balancing losses.

References

Emily Alsentzer, John R Murphy, Willie Boag, Wei-Hung Weng, Di Jin, Tristan Naumann, and Matthew McDermott. Publicly available clinical bert embeddings. *arXiv preprint arXiv:1904.03323*, 2019.

AmirAli Bagher Zadeh, Paul Pu Liang, Soujanya Poria, Erik Cambria, and Louis-Philippe Morency. Multimodal language analysis in the wild: CMU-MOSEI dataset and interpretable dynamic fusion graph. In Iryna Gurevych and Yusuke Miyao (eds.), *Proceedings of the 56th Annual Meeting of the Association for Computational Linguistics (Volume 1: Long Papers)*, pp. 2236–2246, Melbourne, Australia, July 2018. Association for Computational Linguistics. doi: 10.18653/v1/P18-1208. URL https://aclanthology.org/P18-1208/.

Tadas Baltrušaitis, Chaitanya Ahuja, and Louis-Philippe Morency. Multimodal machine learning: A survey and taxonomy. *IEEE transactions on pattern analysis and machine intelligence*, 41(2): 423–443, 2018.

Serhat S Bucak, Rong Jin, and Anil K Jain. Multiple kernel learning for visual object recognition: A review. *IEEE Transactions on Pattern Analysis and Machine Intelligence*, 36(7):1354–1369, 2013.

Ying Cheng, Yang Li, Junjie He, and Rui Feng. Mixtures of experts for audio-visual learning. *Advances in Neural Information Processing Systems*, 37:219–243, 2024.

Zewen Chi, Li Dong, Shaohan Huang, Damai Dai, Shuming Ma, Barun Patra, Saksham Singhal, Payal Bajaj, Xia Song, Xian-Ling Mao, et al. On the representation collapse of sparse mixture of experts. *Advances in Neural Information Processing Systems*, 35:34600–34613, 2022.

Joseph Paul Cohen, Joseph D Viviano, Paul Bertin, Paul Morrison, Parsa Torabian, Matteo Guarrera, Matthew P Lungren, Akshay Chaudhari, Rupert Brooks, Mohammad Hashir, et al. Torchxrayvision: A library of chest x-ray datasets and models. In *International Conference on Medical Imaging with Deep Learning*, pp. 231–249. PMLR, 2022.

Changde Du, Changying Du, Hao Wang, Jinpeng Li, Wei-Long Zheng, Bao-Liang Lu, and Huiguang He. Semi-supervised deep generative modelling of incomplete multi-modality emotional data. In *Proceedings of the 26th ACM international conference on Multimedia*, pp. 108–116, 2018.

William Fedus, Barret Zoph, and Noam Shazeer. Switch transformers: Scaling to trillion parameter models with simple and efficient sparsity. *Journal of Machine Learning Research*, 23(120):1–39, 2022.

Bolin Gao and Lacra Pavel. On the properties of the softmax function with application in game theory and reinforcement learning. *arXiv preprint arXiv:1704.00805*, 2017.

Wenzhong Guo, Jianwen Wang, and Shiping Wang. Deep multimodal representation learning: A survey. *Ieee Access*, 7:63373–63394, 2019.

Xing Han, Huy Nguyen, Carl Harris, Nhat Ho, and Suchi Saria. Fusemoe: Mixture-of-experts transformers for fleximodal fusion. *arXiv preprint arXiv:2402.03226*, 2024.

Hrayr Harutyunyan, Hrant Khachatrian, David C Kale, Greg Ver Steeg, and Aram Galstyan. Multitask learning and benchmarking with clinical time series data. *Scientific data*, 6(1):96, 2019.

Nasir Hayat, Krzysztof J Geras, and Farah E Shamout. Medfuse: Multi-modal fusion with clinical time-series data and chest x-ray images. In *Machine Learning for Healthcare Conference*, pp. 479–503. PMLR, 2022.

Menglin Jia, Luming Tang, Bor-Chun Chen, Claire Cardie, Serge Belongie, Bharath Hariharan, and Ser-Nam Lim. Visual prompt tuning. In *European conference on computer vision*, pp. 709–727. Springer, 2022.

Alistair EW Johnson, Tom J Pollard, Lu Shen, Li-wei H Lehman, Mengling Feng, Mohammad Ghassemi, Benjamin Moody, Peter Szolovits, Leo Anthony Celi, and Roger G Mark. Mimic-iii, a freely accessible critical care database. *Scientific data*, 3(1):1–9, 2016.

Alistair EW Johnson, Lucas Bulgarelli, Lu Shen, Alvin Gayles, Ayad Shammout, Steven Horng, Tom J Pollard, Sicheng Hao, Benjamin Moody, Brian Gow, et al. Mimic-iv, a freely accessible electronic health record dataset. *Scientific data*, 10(1):1, 2023.

Brian Lester, Rami Al-Rfou, and Noah Constant. The power of scale for parameter-efficient prompt tuning. *arXiv preprint arXiv:2104.08691*, 2021.

Victor Weixin Liang, Yuhui Zhang, Yongchan Kwon, Serena Yeung, and James Y Zou. Mind the gap: Understanding the modality gap in multi-modal contrastive representation learning. *Advances in Neural Information Processing Systems*, 35:17612–17625, 2022.

Mengmeng Ma, Jian Ren, Long Zhao, Sergey Tulyakov, Cathy Wu, and Xi Peng. Smil: Multimodal learning with severely missing modality. In *Proceedings of the AAAI Conference on Artificial Intelligence*, volume 35, pp. 2302–2310, 2021.

Saeed Masoudnia and Reza Ebrahimpour. Mixture of experts: a literature survey. *Artificial Intelligence Review*, 42:275–293, 2014.

Basil Mustafa, Carlos Riquelme, Joan Puigcerver, Rodolphe Jenatton, and Neil Houlsby. Multimodal contrastive learning with limoe: the language-image mixture of experts. *Advances in Neural Information Processing Systems*, 35:9564–9576, 2022.

Ronghao Ni, Zinan Lin, Shuaiqi Wang, and Giulia Fanti. Mixture-of-linear-experts for long-term time series forecasting. In *International Conference on Artificial Intelligence and Statistics*, pp. 4672–4680. PMLR, 2024.

Soujanya Poria, Erik Cambria, and Alexander Gelbukh. Deep convolutional neural network textual features and multiple kernel learning for utterance-level multimodal sentiment analysis. In *Proceedings of the 2015 conference on empirical methods in natural language processing*, pp. 2539–2544, 2015.

Wasifur Rahman, Md Kamrul Hasan, Sangwu Lee, Amir Zadeh, Chengfeng Mao, Louis-Philippe Morency, and Ehsan Hoque. Integrating multimodal information in large pretrained transformers. In *Proceedings of the conference. Association for computational linguistics. Meeting*, volume 2020, pp. 2359, 2020.

Chao Shang, Aaron Palmer, Jiangwen Sun, Ko-Shin Chen, Jin Lu, and Jinbo Bi. Vigan: Missing view imputation with generative adversarial networks. In *2017 IEEE International conference on big data (Big Data)*, pp. 766–775. IEEE, 2017.

Noam Shazeer, Azalia Mirhoseini, Krzysztof Maziarz, Andy Davis, Quoc Le, Geoffrey Hinton, and Jeff Dean. Outrageously large neural networks: The sparsely-gated mixture-of-experts layer. *arXiv preprint arXiv:1701.06538*, 2017.

Yuhang Sun, Zhizhong Liu, Quan Z Sheng, Dianhui Chu, Jian Yu, and Hongxiang Sun. Similar modality completion-based multimodal sentiment analysis under uncertain missing modalities. *Information Fusion*, 110:102454, 2024.

Yao-Hung Hubert Tsai, Shaojie Bai, Paul Pu Liang, J Zico Kolter, Louis-Philippe Morency, and Ruslan Salakhutdinov. Multimodal transformer for unaligned multimodal language sequences. In *Proceedings of the conference. Association for computational linguistics. Meeting*, volume 2019, pp. 6558, 2019.

Hu Wang, Yuanhong Chen, Congbo Ma, Jodie Avery, Louise Hull, and Gustavo Carneiro. Multimodal learning with missing modality via shared-specific feature modelling. In *Proceedings of the IEEE/CVF Conference on Computer Vision and Pattern Recognition*, pp. 15878–15887, 2023.

Lean Wang, Huazuo Gao, Chenggang Zhao, Xu Sun, and Damai Dai. Auxiliary-loss-free load balancing strategy for mixture-of-experts. *arXiv preprint arXiv:2408.15664*, 2024.

Qi Wu, Damien Teney, Peng Wang, Chunhua Shen, Anthony Dick, and Anton Van Den Hengel. Visual question answering: A survey of methods and datasets. *Computer Vision and Image Understanding*, 163:21–40, 2017.

Lei Xu, Michael Jordan, and Geoffrey E Hinton. An alternative model for mixtures of experts. *Advances in neural information processing systems*, 7, 1994.

Peng Xu, Xiatian Zhu, and David A Clifton. Multimodal learning with transformers: A survey. *IEEE Transactions on Pattern Analysis and Machine Intelligence*, 45(10):12113–12132, 2023.

Bo Yang and Lijun Wu. How to leverage multimodal ehr data for better medical predictions? *arXiv preprint arXiv:2110.15763*, 2021.

Wenfang Yao, Kejing Yin, William K Cheung, Jia Liu, and Jing Qin. Drfuse: Learning disentangled representation for clinical multi-modal fusion with missing modality and modal inconsistency. In *Proceedings of the AAAI conference on artificial intelligence*, volume 38, pp. 16416–16424, 2024.

Sukwon Yun, Inyoung Choi, Jie Peng, Yangfan Wu, Jingxuan Bao, Qiyiwen Zhang, Jiayi Xin, Qi Long, and Tianlong Chen. Flex-moe: Modeling arbitrary modality combination via the flexible mixture-of-experts. *arXiv preprint arXiv:2410.08245*, 2024.

Amir Zadeh, Rowan Zellers, Eli Pincus, and Louis-Philippe Morency. Mosi: multimodal corpus of sentiment intensity and subjectivity analysis in online opinion videos. *arXiv preprint arXiv:1606.06259*, 2016.

Amir Zadeh, Minghai Chen, Soujanya Poria, Erik Cambria, and Louis-Philippe Morency. Tensor fusion network for multimodal sentiment analysis. *arXiv preprint arXiv:1707.07250*, 2017.

Xinlu Zhang, Shiyang Li, Zhiyu Chen, Xifeng Yan, and Linda Ruth Petzold. Improving medical predictions by irregular multimodal electronic health records modeling. In *International Conference on Machine Learning*, pp. 41300–41313. PMLR, 2023.

Liangwei Nathan Zheng, Chang George Dong, Wei Emma Zhang, Xin Chen, Lin Yue, and Weitong Chen. Devil in the tail: A multi-modal framework for drug-drug interaction prediction in long tail distinction. In *Proceedings of the 33rd ACM International Conference on Information and Knowledge Management*, pp. 3395–3404, 2024a.

Liangwei Nathan Zheng, Chang George Dong, Wei Emma Zhang, Lin Yue, Miao Xu, Olaf Maennel, and Weitong Chen. Revisited large language model for time series analysis through modality alignment. *arXiv preprint arXiv:2410.12326*, 2024b.

Liangwei Nathan Zheng, Zhengyang Li, Chang George Dong, Wei Emma Zhang, Lin Yue, Miao Xu, Olaf Maennel, and Weitong Chen. Irregularity-informed time series analysis: Adaptive modelling of spatial and temporal dynamics. In *Proceedings of the 33rd ACM International Conference on Information and Knowledge Management*, pp. 3405–3414, 2024c.

A Notation

Table 4: Notation

Variable	Definition
E_i	i-th expert function
$\mathbf{E}$	Expert pool
$\mathbf{U}$	ConfNet pool
$\mathbf{h}$	Embedding of arbitrary data input
K	Number of K selection
T	Number of T selection in Post-Imputation
N	Total number of expert
n	Number of instances selected in Pre-Imputation
$G(\cdot)$	Gating function
$\mathbf{g}$	Gating score vector
$\mathcal{H}(\cdot)$	Information entropy
p_t	Confidence of ground truth
$\mathbf{A}_a^*$	Sparse attention map
M_m	Representation of Missing modality m before model backbone
$M_{m,b}$	Modality pool with b instance for M_m
$\bar{M}_m$	Imputed representation of M_m after pre-imputation
M_m^*	Imputed representation of M_m after expert forward and Post-imputation
M_a	Representation of available modality a before model backbone
M_a^k	Representation of M_a returned from k-th expert
M_a^*	Representation of M_a after expert forward
B	Sparsity hyperparameter
b	Number of instance in modality pool
$\|M\|$	Number of modality
$\mathbf{diag}(\cdot)$	Diagonal matrix
δ_{ij}	Kronecker delta
u_i	Softmax logits input at i-th entry
c_i	Confidence score for expert E_i
g_i	Gating score for expert E_i

To facilitate understanding of the model formulation and derivations, Table 4 outlines the notations used throughout this paper. These include variables associated with expert routing, gating mechanisms, modality assignments, and sparsity control, which are central to our proposed ConfSMoE framework.

B Derivation of Jacobian for MoE and Load Balance Loss

B.1 Jacobian for Softmax

This section provides detailed mathematical derivations of the Jacobian matrix used in the gating function of ConfSMoE and its relation to the load balance loss. We first derive the Jacobian of the softmax operation applied to the gating logits, which is essential for analyzing expert selection dynamics. We then extend this analysis to derive gradients of the entropy-based load balance loss. These derivations provide theoretical insights into how sparse expert routing and balanced expert utilization can be jointly optimized.

We first derive the Jacobian of the softmax function as used in the MoE formulation Eq. 2.

$$\mathbf{g} = G(\mathbf{u}) = softmax(\mathbf{u}) = \frac{e^{u_i}}{\sum_{j=1}^{N} e^{u_j}} \tag{11}$$

where u_i is the i-th input value of gate logits.

$$\frac{\partial \mathbf{g}}{\partial \mathbf{u}} = \begin{cases} \dfrac{e^{u_i}(\sum_{j=1}^{N} e^{u_j} - e^{u_i})}{(\sum_{j=1}^{N} e^{u_j})^2} & \text{if } i = j \\ -\dfrac{e^{u_i} e^{u_j}}{(\sum_{j=1}^{N} e^{u_j})^2} & \text{if } i \neq j \end{cases} \tag{12}$$

$$\frac{\partial \mathbf{g}}{\partial \mathbf{u}} = \begin{cases} g_i(1 - g_j) & \text{if } i = j \\ -g_i g_j & \text{if } i \neq j \end{cases} \tag{13}$$

Where g_i represent $\frac{e^{u_i}}{\sum_{j=1}^{N} e^{u_j}}$. This can be further compactly represent as:

$$\frac{\partial \mathbf{g}}{\partial \mathbf{u}} = g_i(\delta_{ij} - g_j) \tag{14}$$

Where $\delta_{ij} = \begin{cases} 1 & \text{if } i = j \\ 0 & \text{if } i \neq j \end{cases}$ is Kronecker delta and the matrix form is:

$$\mathbf{J}_{softmax} = \frac{\partial \mathbf{g}}{\partial \mathbf{u}} = \textbf{diag(g)} - \mathbf{g}\mathbf{g}^\top \tag{15}$$

B.2 Jacobian for Load Balance Loss

Assumption 1 *For any load balance loss $\mathcal{L}_{load}$ applied to a Softmax-based MoE, the effect of $\mathcal{L}_{load}$ is to encourage a flat expert selection distribution, which is equivalent to maximizing the entropy of the gating scores.*

With **Assumption** 1, We have load balance loss $\mathcal{L}_{load} = \frac{1}{\mathcal{H}(\mathbf{g})}$, where $\mathcal{H}(\mathbf{g}) = -\sum_{i=1}^{N} g_i log(g_i)$ is the entropy of the gating distribution.

By applying the chain rule, we obtain:

$$\frac{\partial \mathcal{L}_{load}}{\partial \mathbf{u}} = -\frac{1}{\mathcal{H}(\mathbf{u})^2} \frac{\partial \mathcal{H}}{\partial \mathbf{u}} = -\frac{1}{\mathcal{H}(\mathbf{u})^2} \frac{\partial \mathcal{H}}{\partial \mathbf{g}} \frac{\partial \mathbf{g}}{\partial \mathbf{u}} \tag{16}$$

The intermediate gradients are given by:

$$\frac{\partial \mathcal{H}}{\partial \mathbf{g}} = -log(\mathbf{g}) - \mathbf{g}\frac{1}{\mathbf{g}} = -log(\mathbf{g}) - 1, \quad \frac{\partial \mathbf{g}}{\partial \mathbf{u}} = \textbf{diag(g)} - \mathbf{g}\mathbf{g}^\top \tag{17}$$

Therefore, he final Jacobian of the load balance loss J_{load} is:

$$\mathbf{J}_{load} = \frac{\partial \mathcal{L}_{load}}{\partial \mathbf{g}} = \left[\frac{1}{\mathcal{H}(\mathbf{g})^2}(log\mathbf{g} + 1)^\top\right] \cdot (\textbf{diag(g)} - \mathbf{g}\mathbf{g}^\top) \tag{18}$$

C Experiment Details

C.1 Dataset

MIMIC-III Johnson et al. (2016) is a public dataset contains irregular time series and clinical notes modality. We follow the preprocessing scripts from MMIMI-III benchmark Harutyunyan et al. (2019) and Zhang et al. (2023) to form multimodal patient instance. However, Zhang et al. (2023) filter the instances with missing modality and we modified the scripts to preserve with instances with missing modality. **MIMIC-IV** Johnson et al. (2023) is a public dataset contains irregular time series, clinical notes, ECG signal and chest image. We follow the preprocessing scripts from MedFuse Hayat et al. (2022) to preprocess irregular time series and further preprocess clinical notes, ECG signal and chest image by ourself. We follow the dataset split in MedFuse Hayat et al. (2022) and form multimodal patient instance. **CMU-MOSI** Zadeh et al. (2016) is a multimodal sentiment analysis dataset comprising audio, video, and text modalities. **CMU-MOSEI** Bagher Zadeh et al. (2018) is an extension of the CMU-MOSI dataset, utilizing the same modalities—audio, text, and video from YouTube recordings. We follow preprocessing script of CMU-MOSI and CMU-MOSEI from MMMLMustafa et al. (2022).

C.2 Baselines

SMILMa et al. (2021) impute missing modality with Bayesian meta-learning. **ShaSpec**Wang et al. (2023) leverages multiple loss function to learn the modality-share and modality-specific information and impute the missing modality with modality-shared information. **TF**Zadeh et al. (2017) extract the modality interaction by multimodal sub-networks and tensor fusion layer. **mmFormer**Tsai et al. (2019) is a typical multimodal transformer with multihead attention mechanism. **LIMoE**Mustafa et al. (2022) achieves the multimodal learning with contrastive learning. **FuseMoE**Han et al. (2024) respect the missing modality and jointly learn single and missing modality combination data input and FuseMoE implement Laplacian gating mechanism for modality fusoin and expert selection. In experiment, we denote FuseMoE-S as softmax gating and FuseMoE-L as Laplacian gating. **FlexMoE**Yun et al. (2024) assigns the combination of modality to different experts and impute the missing modality by modality bank. For our approach, we use ConfSMoE-T denotes Token-Level confidence fusion and ConfSMoE-E denotes Expert-level confidence fusion.

C.3 Dataset and Task Description

Table 5: Dataset statistics

Dataset	Task	#Samples	Modality	#Classes	Is Imbalanced?	Missing Ratio
MIMIC-III	48-IHM	6621	Time Series, Text	2	Yes	24.21%
	LOS	6621	Time Series, Text	2	Yes	24.21%
	25-PHE	12,278	Time Series, Text	25	Yes	24.25%
MIMIC-IV	48-IHM	22,733	Image, ECG, Time Series, Text	2	Yes	47.10%
	LOS	22,733	Image, ECG, Time Series, Text	2	Yes	47.10%
	25-PHE	47,027	Image, ECG, Time Series, Text	25	Yes	50.32%
CMU-MOSI	Sentiment Analysis	1870	Audio, Video, Text	3	Yes	0% - 50%
CMU-MOSEI	Sentiment Analysis	20,985	Audio, Video, Text	3	Yes	0% - 50%

48-IHM is a binary classification task, where the time series is truncated to 48 hours readings and predict whether the patient in-hospital mortality in ICU.

LOS is also binary classification task. We formulate task similar to 48-IHM and those patients who spent at least 48 hours in the ICU are filtered to predict the remaining Length Of Stay.

25-PHE is a multilabel classification problem. We attempt to predict one 25 acute care conditions presented in a givem ICU stay record. The definition of those 25 acute care conditions are defined in MIMIC benchmark Johnson et al. (2016)

CMU-MOSI and **CMU-MOSEI** are multimodal sentiment analysis benchmarks consisting of video clips annotated with sentiment scores. Each sample includes aligned audio, video, and text modalities. To simulate modality missingness, we introduce controlled random dropout during training.

All datasets are publicly available and widely adopted in multimodal research. Those datasets can be found and downloaded from the following links:

- CMU-MOSI and CMU-MOSEI download link: https://github.com/zehuiwu/MMML
- MIMIC-III download link: https://physionet.org/content/mimiciii/1.4/ and benchmark: https://github.com/YerevaNN/mimic3-benchmarks
- MIMIC-IV download link: https://physionet.org/content/mimiciv/2.2/ and benchmark: https://github.com/nyuad-cai/MedFuse

C.4 Hyperparameter and Hardware Setting

All experiments are conducted in a remote server with 4 × RTX4090 24 GB with 256 GB RAM and 96-cores CPU.

Table 6: Hyperparameter setting

Parameter	Value
#Expert	8 for MIMIC-III and MIMIC-IV, 4 for CMU-MOSI and CMU-MOSEI
#Top-K Expert	2
Learning Rate	3e-4
Hidden Size	128
#MoE layers	1
Training Epoch	50
Weight for $\mathcal{L}_{conf}$	1
#Top-T for Pre-imputation	10
Random Seed	2023, 2024, 2025
Dropout	0.1

D Other Gating Mechanism

D.1 Mean Gating

The Mean Gate considers the gating score for all experts equally important. Given gating weight $\mathbf{W}_r$, and arbitrary representation $\mathbf{h}$ and gating score $g_i = \frac{1}{N} = [g_1, g_2, \cdots, g_N]$ produced by router $G(\mathbf{u})$, where N is the number of expert.

D.2 Softmax Gating

Given a token embedding $\mathbf{h} \in \mathbb{R}^d$ and there are N expert $E_1, E_2, \cdots, E_N$ with gating scores collected in $\mathbf{g} = [g_1, g_2, \cdots, g_N] \in \mathbb{R}^N$. We introduce a linear weight $\mathbf{W}_r$ to map $\mathbf{h}$ to expert logits $\mathbf{u} = \mathbf{W}_r\mathbf{h} \in \mathbb{R}^N$. As in expert selection, we use softmax to convert the logits to probability distribution:

$$g_i = \frac{\exp(u_i)}{\sum_{j=1}^{N} \exp(u_j)}.$$

D.3 Load Balance Loss

We follow Shazeer et al. (2017) to implement load balance loss used in our experiment.

$$\mathcal{L}_{balance} = \mathbf{CV}^2\left(\sum_{i}^{|D|} importance_i\right) + \mathbf{CV}^2\left(\sum_{i}^{|D|} load_i\right)$$

$$importance_E = \sum_{i}^{|D|} g_i, \quad load_E = \sum_{i}^{|D|} \delta(g_i > 0), \quad \forall E \in \mathbf{E} \backslash E_{top-1}$$

where $CV^2(x) = \left(\frac{\sigma(x)}{\mu(x)}\right)^2$, $\sigma(x)$ is the standard deviation of x $importance_E$ representing the expert importance of E_i and $load_E$. $\delta(\cdot > 0)$ is an indicator function taht is 1 when the inner value is greater than 0. $\mathbf{E} \backslash E_{top-1}$ denotes the set of expert excluding the top-1 selected expert.

D.4 Free-Loss Balance Gating

As the Free-Loss Balance Gating (LFB) Wang et al. (2024) is not officially open-source, we found a github repository that reproduces the implementation: `https://github.com/ambisinister/lossfreebalance`. Formally, the number of instances assigned to each expert $z_i = [z_1, z_2, \cdots, z_i]$ and the average number of instance $\bar{z}$. We introduce a expert-wise bias term $\{b_i\}_{i=1}^{N}$ initialized as zeros and update iteratively in a rule-based manner. This bias term will be added to gating logits $\mathbf{u} = \mathbf{W}_r\mathbf{h} \in \mathbb{R}^N$ of each expert to get a biased gating score u_i^*.

$$u_i^* = u_i + b_i, \quad b_i = b_i + \alpha \times sign(e_i), \quad e_i = \bar{z} - z_i \tag{19}$$

Where, e_i is a load violation error and α is hyperparameter to control the strength of adjustment from violation error. Note that this u_i^* is only used for expert selection in Top-K function instead of expert forward. The gating score g_i used to forward is generated as $g_i = Sigmoid(u_i)$. The authors used sigmoid as they believe the sigmoid achieve slightly better performance than softmax.

D.5 Gaussian Gating

We follow the implementation of FuseMoE Han et al. (2024) for the Gaussian gate baseline. Given a token embedding $\mathbf{h} \in \mathbb{R}^d$ and there are N expert $E_1, E_2, \cdots, E_N$ with gating scores collected in $\mathbf{g} = [g_1, g_2, \cdots, g_N] \in \mathbb{R}^N$. We introduce a matrix of Gaussian gate centers, a learnable parameter denoted as $\mathbf{c} = [c_1, c_2, \cdots, c_N] \in \mathbb{R}^{d \times N}$ for each expert. For a single token, we define the gaussian logits as negative square Euclidean distance $\mathbf{h}$ and each gate center c_i:

$$u_i = -\|\mathbf{h} - c_i\|_2^2, \quad i = 1, \cdots, N.$$

As in expert selection we still use softmax to convert the logits to probability distribution:

$$g_i = \frac{\exp\left(-\|\mathbf{h} - c_i\|_2^2\right)}{\sum_{j=1}^{N} \exp(-\|\mathbf{h} - c_j\|_2^2)}.$$

D.6 Laplacian Gating

We follow the implementation of FuseMoE Han et al. (2024) for the Laplacian gate baseline. Given a token embedding $\mathbf{h} \in \mathbb{R}^d$ and N experts $E_1, E_2, \cdots, E_N$ with gating scores collected in $\mathbf{g} = [g_1, g_2, \cdots, g_N] \in \mathbb{R}^N$, we introduce a matrix of Laplacian gate centers, a learnable parameter denoted as $\mathbf{c} = [\mathbf{c}_1, \mathbf{c}_2, \cdots, \mathbf{c}_N] \in \mathbb{R}^{d \times N}$ for each expert. For a single token, we define the Laplacian logits as the negative Euclidean distance between $\mathbf{h}$ and each gate center $\mathbf{c}_i$:

$$u_i = -\left\|\mathbf{h} - \mathbf{c}_i\right\|_2, \quad i = 1, \cdots, N.$$

As in expert selection, we still use softmax to convert the logits into a probability distribution:

$$g_i s = \frac{\exp(-\left\|\mathbf{h} - c_i\right\|_2)}{\sum_{j=1}^{N} \exp\left(-\left\|\mathbf{h} - c_j\right\|_2\right)}.$$

E Limitation

This work may be limited to expert discontinuity as it is build upon on sparse MoE backbone. A key limitation lies in the dichotomy between fully differentiable MoE and sparse MoE architectures. These two paradigms embody opposite design philosophies, one prioritizing differentiability and comprehensive training, the other emphasizing efficiency through sparsity, making it difficult to simultaneously leverage the benefits of both within a single unified framework.

F Additional Results

These experiments extend the main results presented in Section Experiment and highlight the scalability of our method to real-world multimodal challenges.

Table 7: Experiment setting I: Main results on MIMIC-III

Task	Metric	SMIL	ShaSpec	mmFormer	TF	LlMoE	FuseMoE-S	FuseMoE-L	FlexMoE	**ConfMoE-T**	**ConfMoE-E**
48-IHM	F1	48.56 ± 0.35	34.36 ± 0.73	43.80 ± 0.67	23.09 ± 1.13	47.62 ± 0.21	48.62 ± 0.27	51.63 ± 0.39	47.81 ± 0.31	**53.44 ± 0.27**	50.00 ± 2.17
	AUC	84.00 ± 1.10	79.86 ± 0.53	81.27 ± 0.76	78.47 ± 0.65	83.30 ± 0.64	85.81 ± 0.13	86.22 ± 0.15	85.10 ± 0.61	87.05 ± 0.58	**87.14 ± 0.21**
LOS	F1	62.01 ± 0.54	57.27 ± 0.36	61.10 ± 0.65	56.23 ± 0.79	62.75 ± 0.10	62.26 ± 0.36	62.27 ± 1.61	64.18 ± 0.34	66.27 ± 0.40	**66.39 ± 0.23**
	AUC	80.08 ± 0.35	74.71 ± 0.07	77.94 ± 0.12	72.60 ± 0.79	79.80 ± 0.27	80.05 ± 0.51	79.70 ± 0.43	80.49 ± 0.48	81.66± 0.26	**81.71 ± 0.18**
25-PHE	F1	33.01 ± 0.30	19.52 ± 0.39	35.10 ± 0.38	30.38 ± 0.38	36.22 ± 0.39	33.48 ± 0.22	34.07 ± 0.51	35.31 ± 0.57	37.40 ± 0.13	**40.13 ± 0.40**
	AUC	75.17 ± 1.84	64.61 ± 0.25	71.79 ± 0.26	66.56 ± 0.17	77.93 ± 0.44	77.22 ± 0.29	77.19 ± 0.33	77.37 ± 0.10	**78.93 ± 0.38**	78.28 ± 0.73

Table 8: Experiment setting II: Main results on CMU-MOSI

Missing Rate	Metric	ShaSpec	TF	mmFormer	LlMoE	FuseMoE-S	FuseMoE-L	FlexMoE	**ConfSMoE-T**	**ConfSMoE-E**
0%	F1	41.78 ± 0.64	43.28 ± 0.36	50.22 ± 0.20	50.91 ± 0.19	47.69 ± 0.39	48.15 ± 0.57	51.50 ± 0.55	**51.83 ± 0.27**	51.70 ± 0.29
	AUC	65.08 ± 0.39	64.48 ± 0.51	74.62 ± 0.49	78.12 ± 0.31	75.26 ± 0.20	75.96 ± 0.29	79.38 ± 0.23	80.56 ± 0.10	**80.62 ± 0.07**
10%	F1	43.40 ± 0.74	40.14 ± 0.13	48.66 ± 1.20	49.91 ± 0.33	46.81 ± 0.45	48.81 ± 0.42	49.92 ± 0.28	49.99 ± 0.85	**50.89 ± 0.07**
	AUC	65.45 ± 0.56	61.54 ± 0.66	77.21 ± 0.76	77.12 ± 0.14	70.25 ± 0.93	72.36 ± 0.50	77.07 ± 0.21	**78.06 ± 0.64**	78.03 ± 0.21
20%	F1	39.15 ± 0.13	42.64 ± 0.30	48.51 ± 1.15	48.84 ± 0.61	47.92 ± 0.58	45.00 ± 0.44	49.16 ± 0.24	**50.58 ± 0.73**	50.17 ± 0.31
	AUC	60.87 ± 0.29	65.52 ± 0.98	74.16 ± 0.71	76.64 ± 0.23	71.05 ± 0.36	72.15 ± 0.37	73.80 ± 1.43	77.17 ± 0.55	**77.18 ± 0.11**
30%	F1	39.54 ± 0.17	40.42 ± 0.75	46.66 ± 1.24	46.13 ± 0.55	43.78 ± 0.51	44.48 ± 0.63	45.49 ± 0.44	**47.57 ± 0.10**	47.52 ± 0.77
	AUC	60.80 ± 0.44	60.57 ± 0.99	71.25 ± 0.57	74.33 ± 0.49	70.38 ± 0.56	72.25 ± 0.48	72.54 ± 0.92	**75.59 ± 0.18**	75.42 ± 0.49
40%	F1	35.32 ± 0.32	38.69 ± 0.42	42.22 ± 0.44	43.31 ± 0.38	41.88 ± 0.42	43.20 ± 0.20	43.13 ± 0.61	**45.12 ± 0.27**	44.18 ± 0.10
	AUC	59.58 ± 0.13	61.62 ± 0.07	68.44 ± 0.14	67.21 ± 0.43	64.61 ± 0.63	66.14 ± 0.11	68.12 ± 0.34	**71.65 ± 0.47**	69.55 ± 0.49
50%	F1	36.39 ± 0.97	38.46 ± 1.09	41.14 ± 0.31	41.54 ± 0.77	38.55 ± 0.34	40.90 ± 0.49	41.95 ± 0.48	**44.34 ± 0.77**	42.48 ± 0.12
	AUC	55.60 ± 0.12	60.49 ± 0.80	61.87 ± 0.67	67.43 ± 0.34	62.28 ± 0.28	65.73 ± 0.30	66.47 ± 0.49	**70.41 ± 1.31**	69.04 ± 0.32

Table 9: Experiment setting II: Main results on CMU-MOSEI

Missing Rate	Metric	ShaSpec	TF	mmFormer	LlMoE	FuseMoE-S	FuseMoE-L	FlexMoE	**ConfSMoE-T**	**ConfSMoE-E**
0%	F1	47.48 ± 0.27	38.89 ± 0.54	56.75 ± 0.47	59.13 ± 0.52	57.04 ± 0.15	58.71 ± 0.23	60.62 ± 0.96	61.31 ± 0.14	**62.35 ± 0.12**
	AUC	67.93 ± 0.56	64.26 ± 0.61	76.42 ± 0.24	80.29 ± 0.31	78.54 ± 0.42	78.13 ± 0.34	81.34 ± 0.20	**82.87 ± 0.10**	82.75 ± 0.44
10%	F1	47.41 ± 0.18	34.94 ± 1.10	55.37 ± 0.47	57.46 ± 1.10	55.90 ± 0.55	56.68 ± 0.31	58.66 ± 1.10	59.81 ± 0.34	**60.22 ± 0.31**
	AUC	69.26 ± 0.22	61.05 ± 0.34	75.36 ± 0.53	79.38 ± 0.94	76.38 ± 0.39	76.44 ± 0.12	79.48 ± 0.23	81.00 ± 0.10	**81.05 ± 0.17**
20%	F1	46.54 ± 1.04	35.37 ± 0.94	52.91 ± 0.75	55.35 ± 0.88	54.44 ± 0.27	54.60 ± 0.19	55.96 ± 1.67	**58.06 ± 0.21**	57.66 ± 0.20
	AUC	68.05 ± 0.56	59.54 ± 0.22	73.02 ± 0.65	77.29 ± 0.47	74.32 ± 0.16	74.92 ± 0.64	78.05 ± 0.10	**78.85 ± 0.28**	78.83 ± 0.22
30%	F1	45.05 ± 0.90	35.36 ± 0.84	49.71 ± 0.30	53.93 ± 1.13	52.27 ± 0.35	49.92 ± 0.36	52.00 ± 0.47	54.16 ± 0.49	**54.83 ± 0.15**
	AUC	66.89 ± 0.31	60.23 ± 0.31	71.28 ± 0.10	76.50 ± 0.31	72.22 ± 0.52	72.52 ± 0.29	76.14 ± 0.38	76.91 ± 0.41	**77.10 ± 0.30**
40%	F1	43.49 ± 0.95	32.23 ± 0.61	48.06 ± 0.54	**50.95 ± 0.99**	49.32 ± 0.17	49.36 ± 0.60	49.29 ± 0.28	50.72 ± 0.37	50.66 ± 0.18
	AUC	65.32 ± 0.59	60.09 ± 0.35	69.31 ± 0.10	73.24 ± 0.76	69.85 ± 0.11	70.05 ± 0.46	72.08 ± 1.27	73.63 ± 0.48	**73.88 ± 0.25**
50%	F1	42.75 ± 1.22	33.01 ± 0.51	47.39 ± 0.16	46.69 ± 0.63	43.08 ± 0.47	44.44 ± 0.36	46.19 ± 0.34	47.31 ± 0.20	**48.13 ± 0.33**
	AUC	62.32 ± 0.42	58.20 ± 0.17	66.61 ± 0.22	70.90 ± 0.82	67.63 ± 0.55	67.44 ± 0.16	70.15 ± 1.10	**71.74 ± 0.14**	70.48 ± 0.11

Table 10: Experiment setting III: Main results on CMU-MOSI

Test Modality			Dataset: CMU-MOSI / Evaluation Metric: AUC								
Video	Text	Audio	ShaSpec	mmFormer	TF	LlMoE	FuseMoE-S	FuseMoE-L	FlexMoE	**ConfSMoE-T**	**ConfSMoE-E**
✓	✓		62.18 ± 0.88	72.72 ± 0.08	59.37 ± 1.12	74.63 ± 0.13	55.35 ± 1.11	56.44 ± 1.48	74.59 ± 1.50	**75.57 ± 0.55**	75.56 ± 0.33
✓		✓	55.79 ± 2.53	52.21 ± 0.31	57.87 ± 0.32	56.84 ± 0.34	56.24 ± 1.96	55.11 ± 0.77	52.28 ± 1.23	58.42 ± 0.14	**58.66 ± 0.20**
	✓	✓	65.22 ± 1.01	71.96 ± 0.47	57.89 ± 0.65	75.59 ± 0.39	54.36 ± 1.67	56.10 ± 1.76	75.55 ± 1.64	**77.02 ± 0.63**	76.96 ± 0.64
✓			55.10 ± 1.59	71.01 ± 0.53	58.57 ± 0.44	74.73 ± 0.51	55.94 ± 1.51	55.66 ± 1.66	74.35 ± 1.60	75.07 ± 0.70	**75.11 ± 0.54**
	✓		61.60 ± 4.80	73.77 ± 0.44	60.28 ± 1.42	**75.73 ± 0.33**	55.45 ± 0.95	56.58 ± 1.29	74.42 ± 1.39	75.58 ± 0.55	75.50 ± 0.41
		✓	66.85 ± 3.01	69.04 ± 0.94	57.19 ± 0.72	73.29 ± 0.53	56.04 ± 1.91	57.85 ± 0.74	75.34 ± 1.46	**77.02 ± 0.63**	76.47 ± 0.63

Table 11: Experiment setting III: Main results on CMU-MOSI

Test Modality			Dataset: CMU-MOSI / Evaluation Metric: F1								
Video	Text	Audio	ShaSpec	mmFormer	TF	LlMoE	FuseMoE-S	FuseMoE-L	FlexMoE	**ConfSMoE-T**	**ConfSMoE-E**
✓	✓		41.27 ± 0.81	48.25 ± 0.11	34.96 ± 0.72	44.45 ± 0.33	30.51 ± 2.53	29.90 ± 2.58	50.54 ± 0.73	**54.07 ± 0.29**	54.04 ± 0.36
✓		✓	36.99 ± 2.03	35.79 ± 0.55	34.83 ± 0.54	35.20 ± 0.64	24.29 ± 4.23	27.89 ± 6.23	30.02 ± 7.82	37.40 ± 0.16	**38.17 ± 0.13**
	✓	✓	43.72 ± 1.64	45.53 ± 0.33	37.25 ± 0.53	47.79 ± 0.46	20.68 ± 2.14	29.88 ± 4.55	50.41 ± 1.55	**52.86 ± 0.75**	51.13 ± 0.15
✓			42.98 ± 0.21	46.49 ± 0.91	38.11 ± 0.35	44.86 ± 0.94	25.67 ± 2.82	27.34 ± 2.94	50.39 ± 0.87	53.76 ± 0.43	**54.57 ± 0.35**
	✓		41.36 ± 2.27	47.13 ± 0.54	37.99 ± 0.40	43.81 ± 0.42	25.70 ± 2.82	27.30 ± 2.95	50.65 ± 0.90	**53.77 ± 0.45**	49.93 ± 0.06
		✓	45.45 ± 2.73	46.02 ± 1.21	38.79 ± 0.56	45.50 ± 0.47	25.23 ± 4.59	29.73 ± 3.51	50.57 ± 1.35	**53.72 ± 0.94**	50.69 ± 0.47

Table 12: Experiment setting III: Main results on CMU-MOSEI

Test Modality			Dataset: CMU-MOSEI / Evaluation Metric: AUC								
Video	Text	Audio	ShaSpec	mmFormer	TF	LlMoE	FuseMoE-S	FuseMoE-L	FlexMoE	**ConfSMoE-T**	**ConfSMoE-E**
✓	✓		64.47 ± 0.10	76.60 ± 0.39	56.98 ± 0.20	81.23 ± 0.07	75.81 ± 0.82	76.62 ± 0.37	80.63 ± 0.41	81.45 ± 0.02	**81.52 ± 0.07**
✓		✓	58.41 ± 0.10	56.72 ± 0.84	58.41 ± 0.17	59.64 ± 0.56	57.32 ± 0.62	57.22 ± 0.12	58.28 ± 1.51	**60.33 ± 0.03**	60.00 ± 0.23
	✓	✓	64.46 ± 0.14	75.91 ± 0.04	58.64 ± 0.13	80.00 ± 0.29	77.24 ± 0.60	77.31 ± 0.16	80.00 ± 0.10	**81.26 ± 0.10**	81.23 ± 0.14
✓			63.52 ± 0.19	75.82 ± 0.28	58.71 ± 0.35	80.69 ± 0.34	76.84 ± 0.14	76.27 ± 0.70	81.06 ± 0.20	**81.60 ± 0.13**	81.53 ± 0.22
	✓		64.40 ± 0.24	75.83 ± 0.28	58.89 ± 0.40	80.96 ± 0.26	76.85 ± 0.14	76.51 ± 0.50	80.48 ± 0.21	81.49 ± 0.13	**81.65 ± 0.17**
		✓	65.16 ± 0.04	75.85 ± 0.09	58.32 ± 0.04	80.19 ± 0.11	77.13 ± 0.75	77.23 ± 0.24	80.21 ± 0.11	**81.25 ± 0.10**	81.23 ± 0.14

Table 13: Experiment setting III: Main results on CMU-MOSEI

Test Modality			Dataset: CMU-MOSEI / Evaluation Metric: F1								
Video	Text	Audio	ShaSpec	mmFormer	TF	LlMoE	FuseMoE-S	FuseMoE-L	FlexMoE	**ConfSMoE-T**	**ConfSMoE-E**
✓	✓		40.75 ± 0.14	56.02 ± 0.56	31.38 ± 0.61	58.97 ± 0.53	55.85 ± 0.69	53.59 ± 1.07	60.10 ± 0.76	61.56 ± 0.22	**61.78 ± 0.58**
✓		✓	38.15 ± 0.92	37.12 ± 0.66	31.73 ± 0.16	38.26 ± 2.40	29.40 ± 1.67	33.29 ± 2.89	36.28 ± 3.51	**39.76 ± 0.23**	39.36 ± 1.45
	✓	✓	40.82 ± 0.12	56.06 ± 0.29	31.86 ± 0.23	58.58 ± 0.31	57.02 ± 1.60	53.38 ± 0.65	58.70 ± 2.10	**61.37 ± 0.28**	61.15 ± 0.39
✓			40.37 ± 0.46	55.70 ± 0.35	31.59 ± 0.23	61.20 ± 0.46	54.02 ± 2.88	53.08 ± 0.40	58.58 ± 0.71	**61.84 ± 0.70**	61.78 ± 0.58
	✓		42.16 ± 0.22	55.89 ± 0.37	30.84 ± 0.26	59.35 ± 0.12	55.87 ± 0.68	54.11 ± 0.49	58.42 ± 0.27	61.56 ± 0.61	**61.94 ± 0.37**
		✓	42.45 ± 0.85	56.06 ± 0.29	30.71 ± 0.71	60.00 ± 0.85	56.64 ± 1.65	52.92 ± 1.11	59.50 ± 0.80	**61.10 ± 0.10**	61.00 ± 0.76

Table 14: Control Complexity Study: We control the complexity of model to evaluate performance

Scale	Metrics	ShaSpec	TF	LlMoE	mmFormer	FuseMoE	FlexMoE	ConfSMoE-T
Small	MFLOPs	21,73	4.20	1245.03	237.39	143.93	40.32	39,62
	#Params	2,177,406	2,101,571	2,130,227	2,378,371	20,971,020	2,184,963	2,184,730
	F1 score	39.12 ± 1.21	35.81 ± 0.85	41.11 ± 0.90	41.14 ± 0.31	36.52 ± 0.84	42.12 ± 1.18	44.63 ± 1.65
Medium	MFLOPs	111.27	45.28	6803,84	2830.37	286.02	263.94	268.62
	#Params	11,137,046	11,320,153	11,469,437	11,490,403	11,524,392	11,371,473	11,330,062
	F1 score	41.56 ± 0.67	38.62 ± 0.38	43.21 ± 0.56	42.44 ± 0.79	39.44 ± 0.81	43.78 ± 0.36	45.37 ± 1.73
Large	MFLOPs	331.87	133.47	19668.02	9282,03	308.14	1181.48	1078,82
	#Params	33,203,156	33,368,335	33,000,827	33,428,969	33,182,556	33,385,803	33,398,654
	F1 score	42.82 ± 0.74	37.64 ± 0.88	43.45 ± 0.82	41.50 ± 0.66	40.84 ± 0.67	43.46 ± 1.36	45.55 ± 1.69

G Visualization of Experiment

In this section, we provide visual evidence to further support our claims regarding expert selection dynamics and modality robustness.

Figure 4 shows the UMAP projection of multi-modal embeddings on CMU-MOSI. It clearly demonstrates that imputed modalities form distributions consistent with their original counterparts, suggesting that our imputation module maintains semantic alignment across modalities.

Figure 5 illustrates the softmax gating mechanism without load balance regularization, which exhibits severe expert collapse where only a few experts are consistently selected throughout training. In contrast, Figure 6 shows that our proposed ConfNet gating maintains both load balance and expert specialization, effectively mitigating collapse and enabling more stable and diverse expert routing. We further compared the visualization of our proposed method with Figure 7. SoftMax gating with load balance loss indicate severe ambiguous selection, experts that were heavily selected in one epoch tend to be suppressed in the next epoch. This is a clear empirical result to our gradient analysis that the optimization process of load balance is opposite to learning better routing score. This ambiguous selection, "Sinusoidal Wave" in another word, is also observed in Mean and Gaussian gating as shown in Figure 9 and Figure 11. Mean gating considers all experts equally important and failed to reflect the specification of each expert, resulting suboptimal performance shown in Table 2. By comparing Figure 7 and Figure 9, 11, we observe softmax and gaussian exhibits similar "Sinusoidal Wave" to Mean selection. We can draw a preliminary conclusion that this ambiguous selection, usually leads to suboptimal solution given empirical facts in 2. Moreover, although Laplacian and ConfNet gating are not fully balanced, the "Sinusoidal Wave" exists only to a mild extent and lead to a worth noting performance in 2. All these empirical findings are consistent with our gradient analysis and further support our claim that load distribution should preserve specialization while ensuring a non-trivial load is assigned to less active experts.

Finally, Figures 12 and 13 report and visualize Experiment III results. ConfMoE demonstrates superior resilience across increasing missing rates, with both F1 and AUC metrics degrading gracefully. These results visually confirm the effectiveness of confidence-guided gating and modality imputation under challenging conditions.

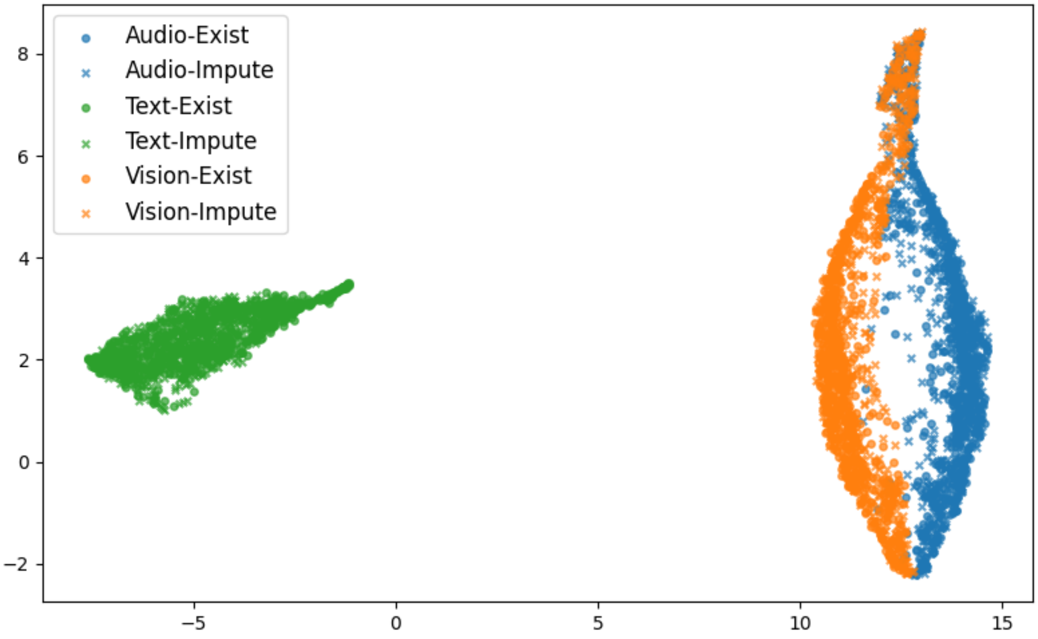

Figure 4: UMAP Visualization of Multi-modal Embedding Space: CMU-MOSI

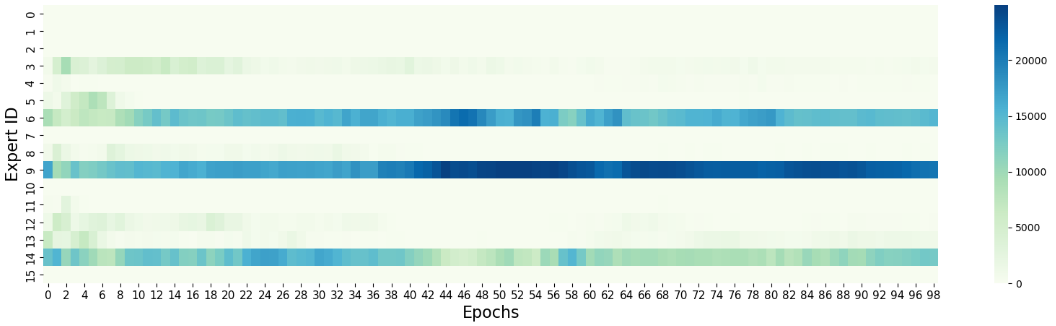

Figure 5: Softmax Score-based without Load Balance Expert Selection: Expert collapse is consistently occurred after epochs 10. While a few certain experts are preferred, this preferred selection becomes worst when the training progresses

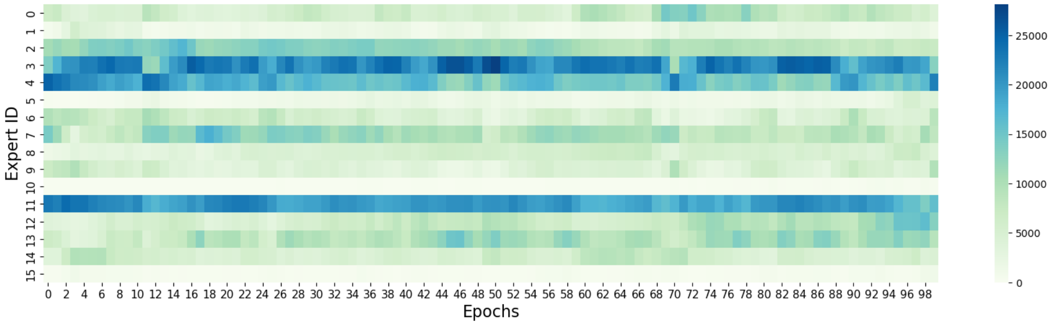

Figure 6: ConfNet Gating Expert Selection: Expert collapse is consistently mitigated throughout training. While certain experts are preferred, less frequently selected experts are still actively utilized. Moreover, expert selection becomes increasingly balanced as training progresses, indicating improved stability and diversity in routing.

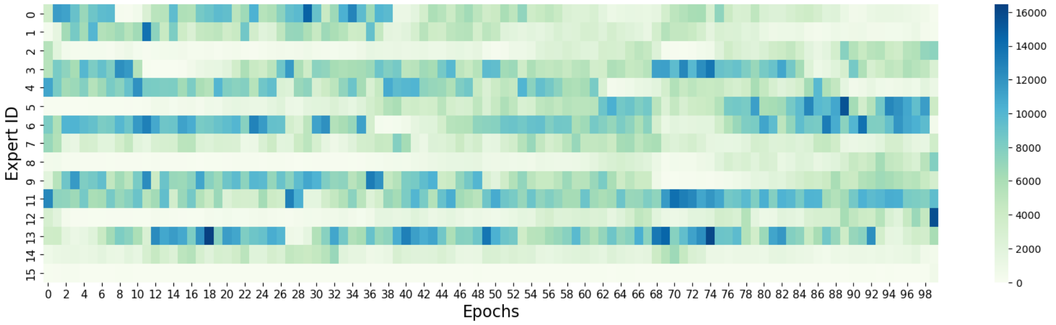

Figure 7: Softmax Gate with Load Balance Loss Expert Selection: An optimization conflict arises, often reflected in a "Sharp Sinusoidal Wave" pattern, experts that were heavily selected in one epoch tend to be suppressed in the next. This oscillatory behavior indicates that the typical load balancing loss does not promote true specialization or expertise among experts. Instead, it merely enforces uniform usage, potentially at the cost of performance, by prioritizing balanced selection over actual expert quality.

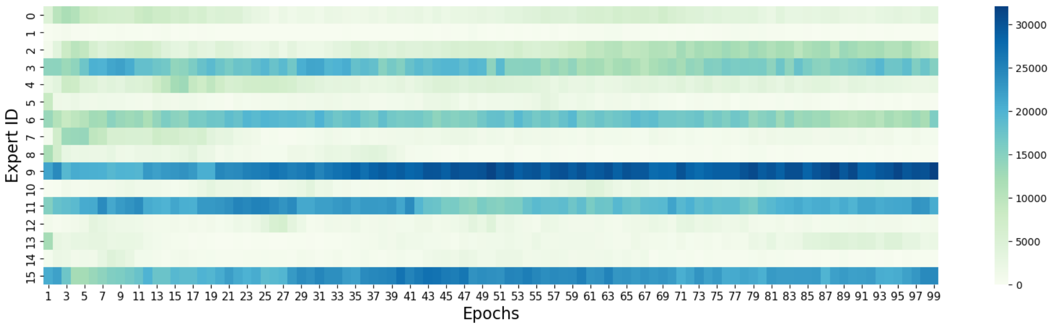

Figure 8: Laplacian Gating Expert Selection: Laplacian gating can partially alleviate the load imbalance issue and achieves better expert utilization than softmax. However, as training progresses, selection becomes increasingly skewed, with only a few experts being consistently chosen. This eventually leads to expert collapse, where most experts become inactive and underutilized.

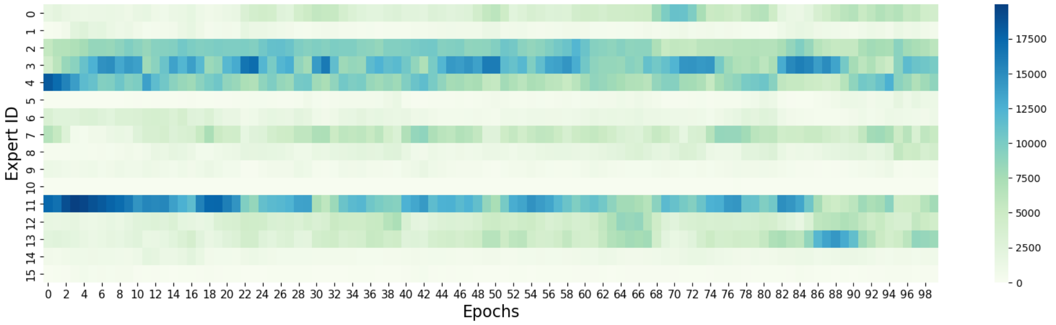

Figure 9: Mean Gating Expert Selection: The "Sharp Sinusoidal Wave" pattern persists under mean gating, where experts heavily selected in one epoch are suppressed in the next. This oscillatory behavior reflects ambiguity in expert selection, stemming from the absence of explicit guidance in the routing mechanism. While mean gating achieves better load balance than Softmax with $\mathcal{L}_{\text{load}}$, it ultimately results in inferior performance, as shown in Table 2.

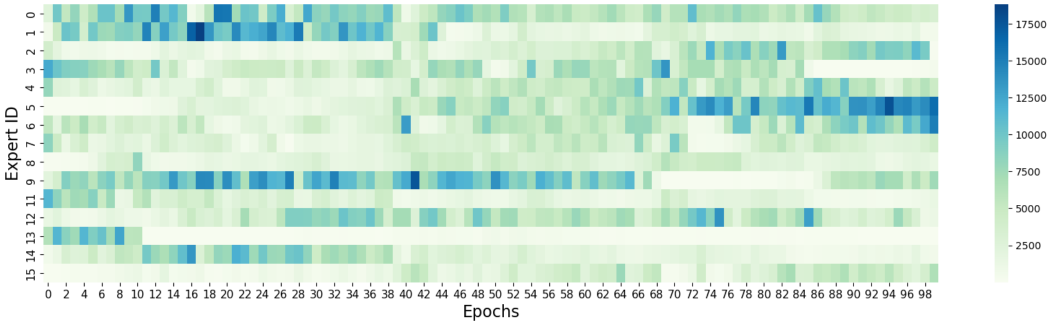

Figure 10: Gaussian Gating Expert Selection: The "Sharp Sinusoidal Wave" pattern persists under Gaussian gating, where experts heavily selected in one epoch are suppressed in the next. This oscillatory behavior reflects ambiguity in expert selection, stemming from the inappropriate gating score guided from Gaussian. While mean gating achieves better load balance than Softmax with $\mathcal{L}_{\text{load}}$, it ultimately results in inferior performance, as shown in Table 2.

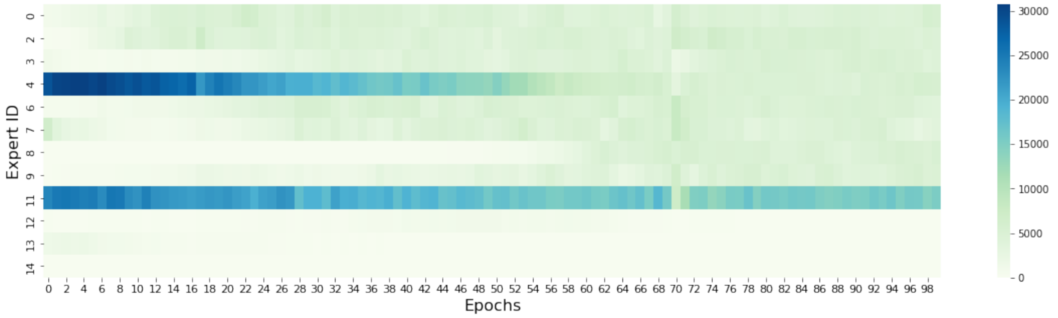

Figure 11: Loss-Free Balance Expert Selection: The "Sharp Sinusoidal Wave" pattern is mitigated under Loss-Free Balance. But this balance technique works too slow as it start balancing load since epoch 50.

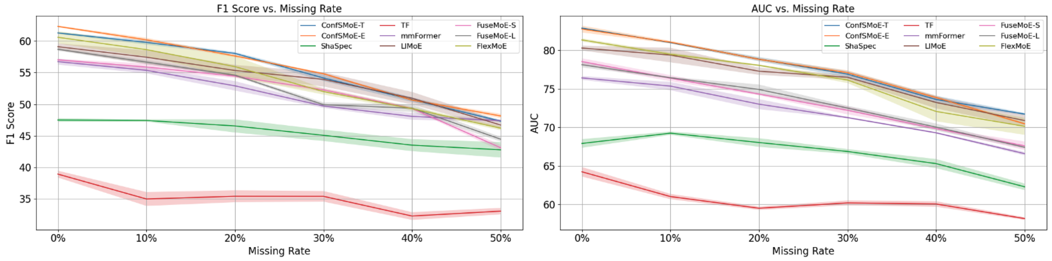

Figure 12: Experiment III: CMU-MOSEI Performance Plot

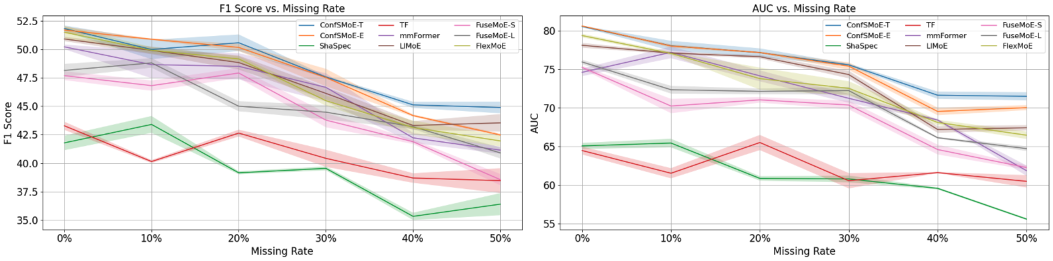

Figure 13: Experiment III: CMU-MOSI Performance Plot

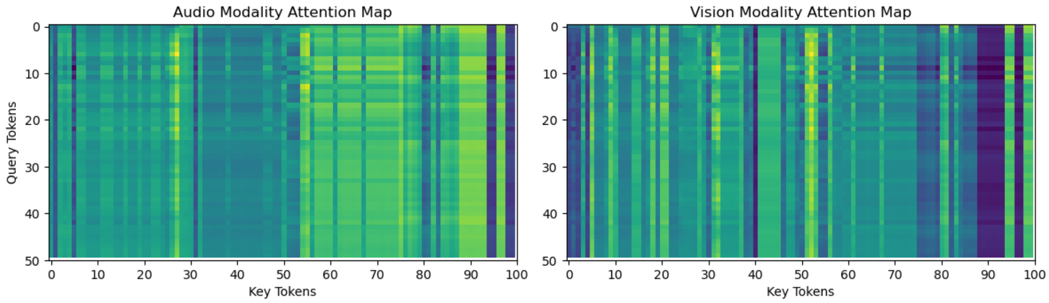

Figure 14: Attention Map from post-imputation: Text as query and Vision, Audio as key. The key tokens are obtained by concatenating tokens from K=2 expert, resulting 100 length of token. The darker the color, the lower attention weight is.

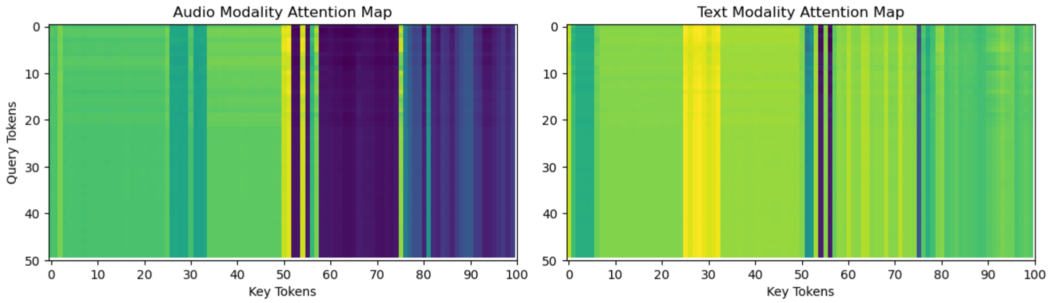

Figure 15: Attention Map from post-imputation: Vision as query and Audio, Text as key. The key tokens are obtained by concatenating tokens from K=2 expert, resulting 100 length of token. The darker the color, the lower attention weight is.

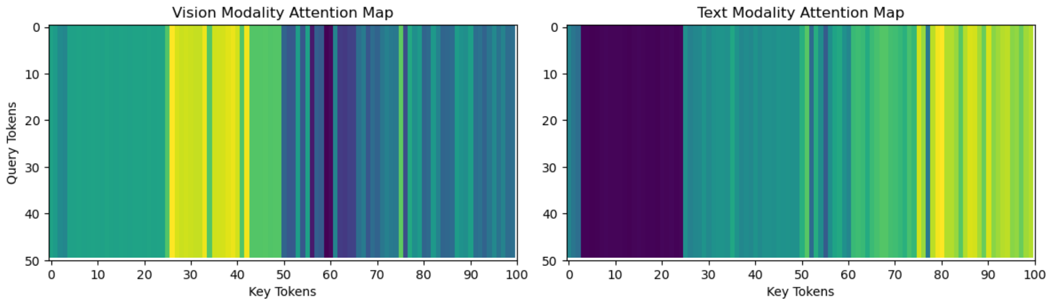

Figure 16: Attention Map from post-imputation: Audio as query and Vision, Text as key. The key tokens are obtained by concatenating tokens from K=2 expert, resulting 100 length of token. The darker the color, the lower attention weight is.

From Figure 14 15 16, we can clearly observed that the attention map are distinctly different when the key are set to different modalities. This indicate that the post-imputation module can dynamically learn, which token are needed depending on characteristics of token and experts. For example, the Figure 16 indicates that 25 - 45th tokens of the first expert are more important than others while the text modalities shows that the second experts are more important. Similar observation are also shows in 14 15 as well. This observation also indicates that modality not only dynamically select information from existing modality but also the specialization of experts. Therefore, we can conclude that the post-imputation can capture expertise of different expert and refine the missing modality accordingly.

H LLM DISCLOSURE

We utilized the ChatGPT language model solely for polishing the writing and refining vocabulary in the *Introduction*, *Proposed Method*, *Results and Discussion*, and *Appendix* sections of this paper. The use of ChatGPT was limited to language editing, and we take full responsibility for the content and interpretations presented in this work.